EFFECT OF CONCENTRATION OF DOPANT STATES ON OPTICAL PROPERTIES AND CRYSTAL STRUCTURE OF NIOBIUM DOPED TiO$_2$

By PAUL AJUOGA
Adm/ No. I/56/7504/04
DEPARTMENT OF PHYSICS

A THESIS SUBMITTED IN PARTIAL FULFILLMENT FOR THE AWARD OF A MASTER OF SCIENCE DEGREE IN PHYSICS AT THE UNIVERSITY OF NAIROBI
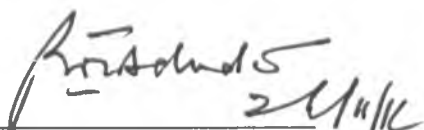
2012

DECLARATION

This thesis is my original work and has not been presented for the award of the degree in any other university.

PAUL AJUOGA

UNIVERSITY OF NAIROBI

This thesis has been submitted for examination with the approval of the following as my university supervisors:
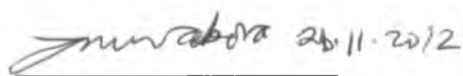
1. Prof. B.O Aduda

   University of Nairobi

   Department of physics

   P.O Box 30197

   NAIROBI

2. Prof. J. M. Mwabora

   University of Nairobi

   Department of physics

   P.O Box 30197

   NAIROBI

ACKNOWLEDGEMENT

ABSTRACT

The optical band gaps, crystal structure, and anatase–to–rutile phase transformation were studied on Nb–doped TiO_2 (concentration range 0.02–0.06 at. % Nb^{5+}) films prepared by high temperature diffusion method. The Nb–doped TiO_2 films displayed a slight yellow colour attributed to O–Nb=O centres and an enhanced visible light absorption with a red shift of 18.2 nm of the optical absorption edge from 394 nm for pure TiO_2 film to 412.2 nm for 0.04 at. % Nb–doped TiO_2 film. This represents a band gap lowering of 0.181 eV due to the donor–type behavior of niobium. As the niobium concentration increased, the enhancement in light absorption at the investigated concentration range goes through a maximum at 0.04 at. % Nb^{5+} with minimum band gap of 3.017 eV and starts to decrease again at 0.06 at. % Nb^{5+} with a band gap of 3.036 eV. The fabricated films exhibited rather low transmittance and reflectance. Despite higher rutilization, at the doping temperature of 850 ^oC used, crystal sizes (39–43 nm) obtained from X–ray diffraction spectra depicted a significant increase in surface areas which is attributed to retardation of exaggerated anatase–rutile phase transformation caused by Nb–doping into the TiO_2 matrix.

TABLE OF CONTENTS

LIST OF ABREVIATIONS

CB	Conduction band
DLTS	Deep Level Transcient Spectroscopy
DUV	Deep Ultraviolet
EDX.RF	Energy Dispersive X–Ray Fluorescence
EHP	Electron–hole–pair
InGaAs	Indium Gallium Arsenide
MCA	Multi–Channel Analyzer
MOCVD	Metalorganic Chemical Vapour Deposition
Nb	Niobium atom
Nb_2O_5	Niobium pentoxide
NIR	Near infra–red
PbS	Lead sulfide
PMT	Photomultiplier
Pt	Platinum
Ti	Titanium atom
TiO_2	Titanium dioxide
UV	Ultra–violet
VB	Valence band
VIS	Visible Spectrum

LIST OF SYMBOLS

Å	Angstrom unit
a	Anatase phase
B	Edge width parameter
d	Depletion region width
D^{m+}	Dopant with valency m+
e^-	Free electron
e	Naperian base
e^-/h^+	Electron-hole pair
E_{cb}	Conduction band edge
E_{Fm}	Equilibrium Fermi level of metal
E_{Fs}	Equilibrium Fermi level of film
E_g	Band gap energy
E_i	Intrinsic level
E_{redox}	Redox potential of water
eV	Electron volt
E_{vb}	Valence band edge
h	Planck's constant
$\hbar$	Planck's constant divided by 2π
I	Light intensity
I_A	Anatase phase x-ray intensity
I_R	Rutile phase x-ray intensity
l	Penetration depth of light
n	Refractive index
n_s	Refractive index of the film
Nb4d	Niobium 4d-orbital
Nb^{5+}	Niobium ion
O_{2p}	Oxygen 2p-orbital
R	Optical reflectance
r	Rutile phase
t	Film thickness
T	Optical transmittance
Ti3d	Titanium 3d-orbital
Ti^{4+}	Titanium ion

$T_{normalized}$	Normalized transmittance data
x	Direction of wave propagation
v	Linear frequency of electromagnetic light wave
a_o	Radius of the hydrogenic wave function of a trapped carrier
$I(x)$	Light intensity at penetration depth x
I_o	Incident light intensity
I_{s1}	Light intensity just inside the semiconductor
I_{s2}	Light intensity at the lower end of the semiconductor
$K_{recom.}$	Tunneling recombination
$M^{(m+1)}$	Metal ion with hole trap
$M^{(m-1)}$	Metal ion with electron trap
M^{m+}	Metal ion
$R_{(\lambda)}$	Reflectivity of a medium
R_1	Fresnel power reflection coefficient
R_2	Fresnel reflection at semiconductor–substrate interface
R_3	Fresnel reflection at substrate–air interface
$R_{e-/h+}$	Electron/hole pair separation distance
S	Substrate surface
$T(E)$	Optical transmittance through the film
Ta^{5+}	Tantalum ion
W^{6+}	Tungsten ion
$\alpha(E)$	Coefficient of absorption
δ	Conductivity
λ	Wavelength
λ_g	Threshold wavelength

LIST OF FIGURES

LIST OF TABLES

CHAPTER ONE

INTRODUCTION

1.1 Introduction

Research on titanium dioxide light absorption has for the past four decades attracted considerable attention for possible broad applications in solar cells, photocatalysis, gas sensors, etc. However, the wide band gap of TiO_2 (3.0 eV and 3.2 eV for rutile and anatase respectively) means that only UV light excites electrons over the band gap. In many applications, including those utilizing solar light as the energy source, it is therefore desirable to extend the band gap excitations into the visible region in order to exploit a larger portion of the spectrum. Several methods and materials have been attempted. These include the use of dopants such as anion doping where the lattice oxygen is replaced with nitrogen (Lindgren *et al*, 2003; Diwald *et al*, 2004, and Valentin *et al*, 2004), carbon (Wang and Lewis, 2005), fluorine (Hattori *et al*, 1998; Ayllon *et al*, 2000; Todorova *et al*, 2007), sulphur (Asahi *et al*, 2001; Umebayashi *et al*, 2002; 2003a) and cation doping in which Ti cations are substituted with metals such as vanadium, ruthenium, manganese, iron, tungsten, niobium, etc, atoms (Karakitsou and Verykios, 1993; Wang *et al*, 1994). Other possible visible active materials include binary oxides and perovskites (Martson *et al*, 2006).

Several investigators have tried to explore the potential of using niobium doped TiO_2 as a visible photoactive material for different applications in photocatalysis (Karakitsou and Verykios, 1993), solar cells (Wang *et al*, 1994; Trenczek–Zajac *et al*, 2007), air and water pollution control (Martson *et al*, 2006), gas sensing (Feroni *et al*, 2000; Yamada *et al*, 2000 and Ruiz *et al*, 2003), maintenance free surfaces (Radecka and Rekas, 1995), etc.

Niobium oxide, and in particular its most stable form Nb_2O_5, is a semiconductor with a band gap of about 3.9 eV (decreasing to about 3.5eV in the amorphous state), with a high dielectric constant and a high index of refraction. It has found many uses in electronic and optical applications (Sehmitt and Aegarter, 2000; Martson *et al*, 2006). In recent findings (Martson *et al*, 2006) it was shown that Nb–doped anatase produces films with high electron conductivity which finds useful applications in certain photochemical systems.

It is a delicate process to introduce Nb–dopant impurity into TiO_2 in order to alter both its optical characteristics and subsequent band gap. This is because the doping parameters must be carefully chosen so as to avoid creation of unwanted recombination centres which prevent efficient separation of photo–excited electron–hole pairs (Andreas *et al*, 2006). The development of new Nb–doped TiO_2 photoelectrodes for use in solar cells, gas sensing, photocatalysis, etc, is needed while at the same time addressing the disadvantages of their low efficiencies and long–term instability caused by chemical reactions with ambient (such as oxygen, water vapor and other gases).

Efforts are being made to fabricate TiO_2 photoelectrodes for the utilization in solar energy devices (Grätzel and O'Regan, 1991; Grätzel, 2003), gas sensors (Feroni *et al*, 2000), photocatalysis (Karakitsou and Verykios, 1993), etc, at a cheaper cost but with improved efficiencies.

In nanostructured TiO_2, semiconducting films with high structural modifications, the electrical conductivity and other optical characteristics are determined by defects in the lattice structure, presence of dopants and by the features of the percolative network formed by the grains (Feroni *et al*, 2000). In the present study, we attempt to fabricate nanostructured Nb–doped TiO_2 thin films prepared via high temperature diffusion and explore its possible utility in photochemical applications. The effect of concentration of Nb–dopant states on the optical properties and crystal structure of polycrystalline Nb–doped TiO_2 will be studied.

1.2 Statement of the Problem

TiO_2 is an n–type semiconductor and doping it with cations of valence higher than that of the parent Ti^{4+} cation such as niobium ion (Nb^{5+}), results in increased concentration of electrons in the conduction band due to the donor–type behavior of niobium. In previous studies, niobium has been found to inhibit anatase–to–rutile phase transformation at high temperatures (Otshuka *et al*, 1982) while at the same time contrasting opinion by various studies as to whether niobium dopes interstitially or substitutionally into the TiO_2 lattice still persists (Arbiol *et al*, 2002; Martson *et al*, 2006). Recent studies on niobium doping in TiO_2 are focused on optimizing the photo–response of TiO_2 by employing a wide range of niobium concentrations (at

2

mmol. and mol. % Nb.) together with different doping techniques. One of the cheapest and most common techniques used to introduce Nb^{5+} ions in the TiO_2 matrix is high temperature diffusion. The mechanisms of how niobium doping at various concentrations and temperatures modify the structural, electrical, chemical and optical properties of TiO_2 for possible technological applications still need to be understood. This will allow us to define more precisely the most suitable range of compositions and thermal treatments which give the best results for envisaged applications if niobium doping route is to mature into a viable commercial technology.

1.3 Objectives of the Study

The aim of the present study is to optimize the niobium–doped TiO_2 visible light absorption with a view to increasing its utility for applications in devices. The specific objectives are:

1. Fabrication of niobium–doped TiO_2 thin films of niobium concentration range of 0.02–0.06 at. % via high temperature diffusion.
2. Studying the optical characteristics such as transmittance, reflectance and band gap of the fabricated niobium–doped T_iO_2 films.
3. Studying the structure and composition of the fabricated niobium–doped TiO_2 films.

1.4 Justification and Significance of the Study

The present study is mainly devoted to investigating how the variations of very low concentrations of niobium (0.02–0.06 at. %) in TiO_2 influences its optical properties and structural characteristics. This knowledge is useful in fabricating new Nb–doped TiO_2 photoelectrodes for possible use in gas sensors, solar cells, environmental degradations caused by organic pollutants, degrading toxins produced algae, etc. It is also hoped that the study will provide impetus for further investigations in Nb–doped TiO_2 thereby contributing to the first growing scientific body of knowledge.

CHAPTER TWO
LITERATURE REVIEW

2.1 Introduction

Titanium dioxide (TiO_2) belongs to one of the most extensively investigated semiconducting oxide materials for various applications. This is because it has the advantages of being inexpensive, chemically stable and non–toxic. Titanium dioxide is a multifaceted compound. It is used for photovoltaic, photocatalysis, gas sensing, maintenance–free surfaces and humidity detection applications as it combines good electrical properties with excellent stability in many solvents over a wide pH range (Oliver *et al*, 2004). It also makes tooth pastes white and paint opaque. In photocatalysis application, it is a potent photocatalyst that breaks down almost any organic compound when exposed to sunlight. This photocatalytic property has been used in developing a wide range of environmentally friendly products including self–cleaning fabrics, autobody finishes (super hydrophilic surfaces), ceramic tiles, paving stones, degrading toxins produced by blue–green algae, removing the ripening hormone ethylene from areas where perishable fruits, vegetables and cut flowers are stored (Fujishima *et al*, 2000; Soonchul *et al*, 2008) as well as organic pollutants such as trichloroethylene and methyl–tert–butyl ether from water (Qamar *et al*, 2006).

Despite the broad range of applications of TiO_2 only about 4% of the solar spectrum (ultraviolet) can be utilized due to its wide intrinsic band gap (3.0 eV for rutile and 3.2 eV for anatase phases), i.e., a fundamental absorption edge of about 400 nm (Grätzel and O Regan, 1991; Karakitsou and Verykios, 1993; Wang *et al*, 1994; Choi *et al*, 1994). Both rutile and anatase crystalline phases are transparent to visible light (Karvinen, 2003). Rutile is preferred in paint and pigmentary industry as well as high temperature gas sensing because it scatters light more efficiently and is more stable at higher temperatures than anatase. But for photoelectrochemical solar cell applications, anatase thin film is preferred because of its unique combination of high refractive index (n=2.5) with high degree of transparency in visible region of the spectrum (Smestad, 1998; Karvinen, 2003). In its colloidal form, anatase structure also shows high mobility of n–type charge carriers (Sodergren *et al*, 1994; Fujishima *et al*, 2000).

Considerable efforts have been made to extend the photo–response of TiO_2 based system further into the visible region using dopants (Kerakitsou and Verykios, 1993;

Choi *et al*, 1994; Wang *et al* 1994; Radecka & Rekas, 1995; Umebayashi *et al*, 2003b; Oliver *et al*, 2004; Christiana *et al*, 2004; Wang and Lewis 2005; Trenczek–Zajac *et al*, 2007). Various transition metal cation doping of TiO_2 have been intensively attempted. Cation–metal doping implies incorporation of a foreign cation into the crystal lattice of the parent semiconductor metal oxide. The electronic structure of the parent semiconductor is altered in a systematic manner by employing doping cations of lower, equal or higher valence than that of the parent cation. By selective cation metal doping the properties of TiO_2 colloids and electrodes are modified and their interfacial charge transfer reactions are enhanced. However, the disadvantage of cationic dopants is that most of them result in localized d–levels deep in the band gap of TiO_2 which serve as recombination centres for photogenerated charge carriers (Wang and Lewis, 2005)

2.2 Effect of Doping TiO_2

The photoreactivity of doped TiO_2 is a complex function of dopant concentration, the energy level of the dopants, ionic/atomic radius of the dopants and the electronic configurations and the light intensity. Even though the microscopic motion of atoms from one site to another may be rather complex, possibly involving vacancies, interstitial and substitutional positions, atomic exchanges and others, the basic description of the effective diffusion remains governed by Fick's first and second laws (Boer, 1991). The relative efficiency of a metal ion dopant depends on whether it serves as a mediator of interfacial charge transfer or as a recombination center. Enhanced interfacial charge transfer in the presence of effective dopants appears to be the most important factor in the enhancement of the photoreactivity of doped TiO_2 (Choi *et al*, 1994).

Introduction of metal ion impurity levels into the TiO_2 band gap induces a red shift in the band gap transition and the visible light absorption through a charge transfer between a dopant and conduction band (CB) or valence band (VB) or a d–d transition in the crystal field (Mizushima *et al*, 1979). Gratzel, 1983, showed that some transition metal ion–doped TiO_2 samples at different dopant concentrations have an optimal concentration of 0.5 at. % for enhanced photoreactivity and this observation was found to be consistent with their transient absorption spectrum, Choi *et al*, 1994 reported that doping TiO_2 with trivalent or pentavelent metal ions was detrimental to

its photocatalytic activity. They proposed a general photochemical charge–trapping, recombination, detrapping and migration mechanisms in the presence of metal ion dopants. They attributed the inhibition of e^-/h^+ recombination in some transition metal ion–doped TiO_2 colloids to the local separation of trapped charge carriers. However, except for a few cases, the photoreactivities of most transition metal ion–doped TiO_2 decrease even in the UV region (blue shift). This is because the transition–metal–doped TiO_2 suffers from an increase in carrier recombination centres introduced by the dopant–related localized d–states deep in the band gap of TiO_2 or thermal instability at higher temperatures, usually above 800 °C.

Karakitsou and Verykios, 1993 noted that doping TiO_2 with (D^{m+}), m>4 (where D^{n-} is the dopant with valency m+) increased the capacity of the TiO_2/substrate space charge region to separate photogenerated electron–hole pairs and to reduce recombination. As the m–dopant concentration increases, the surface barrier becomes higher and the space charge region narrower. The electron–hole pairs photogenerated within the region are efficiently separated by the large electric field traversing the barrier before having the chance to recombine. Since the space charge region is very narrow, the penetration depth of light into TiO_2 greatly exceeds the barrier width. Hence a fraction of incident light generates electron–hole pairs in the bulk of the semiconductor, which is field–free, and the carriers easily recombine (this fraction of light does not contribute to photoreactivity). Thus a value of m–dopant concentration at which the widths of the surface barrier have an optimal value exists with a corresponding maximum rate of photoreactivity which depicts an extension of the absorption edge to lower energy into the vsible light region.

Metal ion dopants influence the photoreactivity of TiO_2 by acting as electron (or hole) traps and by altering the e^-/h^+ pair recombination rates through the following process.

$$M^{m+} + e^-_{cb} \longrightarrow M^{(m-1)+} \text{ electron trap} $$
$$M^{m+} + h^+_{vb} \longrightarrow M^{(m+1)+} \text{ hole trap} \quad \Big\} \quad \cdots\cdots\cdots (2.1)$$
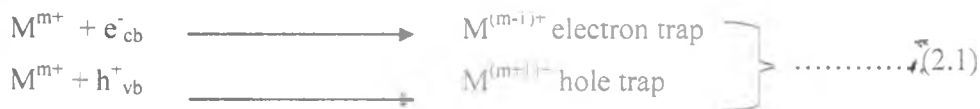
where the energy level for $M^{m+}/M^{(m-1)}$ lies below the conduction band edge (E_{cb}) and the energy level for $M^{m+}/M^{(m+1)}$ above the valence band edge (E_{vb}) (Choi *et al*, 1994). Choi *et, al* 1994 further noted that there appears to be an optimal dopant concentration

above which photoreactivity decreases due to change in space charge layer thickness. The recombination ($K_{recom.}$) through tunneling between the trapped charge carriers depends on the distance ($R_{e-/h+}$) separating the e^-/h^+ pair according to:

$$K_{recom.} \propto \exp(-2R_{e-/h+}/a_o) \dots\dots\dots\dots\dots\dots\dots\dots\dots\dots\dots\dots\dots\dots(2.2)$$

where a_o is the radius of the hydrogenic wave function of the trapped carriers. Hence the recombination rate increases exponentially with the dopant concentration as the average distance between trap sites decreases with increasing number of dopants confined within a particle. At lower concentrations below the optimal value, photoreactivity increases with an increasing dopant concentration because there are fewer trapping sites available. Martin *et al*, 1997, observed that charge transfer of trapped charge carriers to a redox couple at the interface is a very slow process, which might be extended up to a second especially at higher light intensities. This indicates that the dopants are efficient recombination centres as well as good trapping sites. They further concluded that metal ion dopants act as effective trapping sites under low light intensities (below UV) when not all the dopants sites are populated as traps. However, when the available trapping sites are fully occupied under conditions of high light intensities (UV) the metal ion dopants become efficient recombination centres.

Anpo *et al*, 1998, reported that transition metal ion implantation into TiO_2 shifts the absorption edge to lower energies, thereby increasing its photo–response in the visible region. Previous experimental and theoretical studies concerned with the transition metal doped TiO_2 consistently indicate that the energy level and d–electron configuration of the dopant govern the photoelectrochemical process in the visible regions (Choi *et al*, 1994; Umebayashi *et al*, 2002). The surface chemistry, crystal structure and size and crystal defects of TiO_2 depend on both preparation methods and presence of impurities in the sample (Karvinen, 2003).

In earlier studies, Karakitsou and Verykios, 1993, showed that doping with cations of valence higher than that of Ti^{4+} such as tungsten ion (W^{6+}), tantalum ion (Ta^{5+}), niobium ion (Nb^{5+}), etc into TiO_2 matrix results in enhanced photoreactivity. The

7

enhancement or reduction of photoreactivity of TiO_2 is also dependent on the concentrations of the doping cations. These cations alter the bulk electronic structure of TiO_2 which influences its electron–hole pair generation and separation capacity under illumination in order to initiate oxidation–reduction reactions for conversion of solar to chemical energy. Such higher valence doped TiO_2 were also found to exhibit enhanced electrical conductivity and reduced activation energy of electron conduction. They found that although appreciable doping of these cations had taken place at the calcination temperature of 900 ^{o}C, the enhanced photoreactivities at 0.11 at.% W^{6+}, 0.12 at.% Ta^{5-}, 0.2 at.% Nb^{5+} were still minimal for any appreciable utility of the doped TiO_2 photoelectrodes.

Several approaches have been used to improve the photo-efficiency of TiO_2 semiconductors. One of the popular methods is doping with substitutional elements such as niobium. Otshuka et al, 1982, noted that pentavelent doping of TiO_2 with niobium shifted solar spectral absorption edge to lower energy. Cation dopants such as niobium ion (Nb^{5+}) of valence higher than that of the parent cation (Ti^{4+}) had been found to alter the electronic structure of TiO_2, i.e., additional energy levels (deep or shallow) are created within the band gap of TiO_2 (Karakitsou and Verykios (1993). These additional states (energy levels) influence its electron–hole pair generation and separation capacity under solar illumination in order to initiate oxidation–reduction reactions for conversion of solar to chemical energy. Wang et al, 1994, found that Nb–doping into TiO_2 matrix shifts the optical absorption edge towards the visible light region as well as improve the photocurrent density of TiO_2. But, they further concluded that although the enhancement of photocurrent density and quantum efficiency resulting from niobium addition in TiO_2 had been studied for many years, the improvement still seemed too little for Nb–doped TiO_2 to be used in practice.

Niobium is an example of a shallow dopant and so acts as a mediator of interfacial charge transfer, hence it does not act as a recombination center (Karvinen, 2003). Such a shallow level dopant is intimately connected with adjacent conduction band of TiO_2, and therefore has quasi–hydrogen like model described by eigenstates (see Fig. 3.4) (Umebayashi et al, 2003b). This makes it a good scattering center (Boer, 1991). However, recent studies by Miyagi et al, 2004, on Nb-doped anatase TiO_2 epitaxially grown on $SrTiO_3$ by metalorganic chemical vapour depositions (MOCVD), using

deep level trancient spectroscopy (DLTS) revealed that Nb ions produce not only shallow dopants but also at least two kinds of deep levels in anatase TiO_2 (0.3 eV and 0.67 eV) below the bottom of the conduction band. This is due to the splitting of the upper and lower conduction bands. Recent studies by Martson *et al*, 2006, on nanostructured Nb–doped TiO_2 (10–20 mol% Nb_2O_5) gave an inferior photoreactivity attributed to an enhanced electron–hole pair recombination rate due to the Nb=O cluster and cation vacancy formation. Despite the fact that Nb–doping extends the optical absorption into the visible spectrum, their result showed that Nb–doped TiO_2 with such high Nb–dopant concentration is a poorer photoactive material than pure TiO_2.

Studies by Bonini *et al*, 2000, Arbiol *et al*, 2002, and Ruiz *et al*, 2003, on Nb–doped TiO_2 nanopowders (Nb contents 0–10 at.%) found that Nb–doping introduced electronic states at the surface or into the bulk that modify the base material's electrical conductivity. This is because niobium, acting as a donor dopant reduces the electrical resistance of TiO_2 while at the same time maintains its usual n–type behaviour. Yamada et al, 2000, pointed out that Nb–doping increases the n–type carrier concentration and their mobility since majority of electronic carriers are alternated from p–type to n–type according to the amount of niobium introduced in TiO_2. However, their estimations on Nb–doped TiO_2 film resistance suggested that it appears only part of niobium behaves as electron donor while others remain as neutral states.

Niobium addition into TiO_2 had been found to considerably lower the average grain size in Nb–doped TiO_2, by retarding anatase–rutile phase transformation at temperatures as high as 800 °C (Feroni *et al*, 2000). However, other studies have obtained anatase–to–rutile phase transition onset temperature as low as 700 °C and others as high as 1200 °C depending on doping method employed, type of electrodes (e.g., pellets or films) to be fabricated and substrates (e.g., Al_2O_3, silicon, glass, etc) used (Wang*et al*, 1994; Madare *et al*, 2000: Yamada et al, 2000; Trenczek–Zając *et al*, 2007). Although niobium doping suppresses grain growth, prolonged doping time (> 10 hours) at higher temperature increases niobium segregations (Karvinen, 2003).

Various investigations have been conducted on non–metal–doped TiO_2 films with the aim of improving their photo–response into the visible spectrum. Asahi *et al*, 2001, proposed a narrowing of the TiO_2 band gap due to mixing of N2p states with O2p states in the valence band of N–doped TiO_2. However, Christiana *et al*, 2004, suggested that because of different structures and densities, N–doping has opposite effects on the photoreactivity of anatase and rutile TiO_2 leading to a red shift and a blue shift respectively of the optical absorption band edge. Oliver *et al*, 2004, in their investigation also found out that for N–doped TiO_2, interstitial dopants are active for lowering the photochemical threshold energy below the band gap energy of TiO_2. Although the related nitrogen–impurity states are close to the TiO_2 valence band maximum, contrasting scientific opinions are still obtained by these studies depending on the doping methods employed. Lindgren *et al*, 2003, in their investigation on substitutional nitrogen in the form of nitride species obtained a shift of the photo–threshold energy to higher energy due to nitrogen doping compared to un–doped TiO_2.

Hebenstreit *et al*, 2001, incorporated sulphur into TiO_2 by oxidation of TiS_2 and discussed the doping effect on its optical–response properties, and their study showed that sulphur doping into the TiO_2 lattice contributes to band gap narrowing caused by the overlap of the split sub–levels of the $2p_{3/2}$ and $2p_{1/2}$ states with separation of 1.2 eV by spin orbit coupling. Further studies by Umebayashi *et al*, 2002, concluded that substitution of sulphur (S) for oxygen in TiO_2 could cause a significant shift in the absorption edge to lower energy. Their analysis using the *ab initio* band calculations showed that band gap narrowing due to S–doping originated from mixing the S3p states with valence band (VB) width. This is because when TiO_2 is doped with sulphur, the S3p states are somewhat delocalized, thus greatly contributing to the formation of the VB with the O2p and Ti3d states. Consequently, the mixing of the S3p states with the VB increases the width of the VB itself, and these results in a decrease in the band gap energy due to sulphur doping. A further investigation by the same group in 2003 (Umebayashi *et al*, 2003) on the S–doped TiO_2 prepared by ion implantation method followed by analysis of its photo–electronic response and electronic structure using photocurrent spectroscopy and first principle band calculations resulted in the conclusions that:

(i)   In the S–doped TiO_2 the photo–to–carrier conversion occurred in the visible light region above 420 nm (< 2.9 eV).

(ii)   S–doping into TiO_2 causes an increase in the width of the valence band, thus resulting in band gap narrowing.

In contrast, these observations did not highlight the percentage concentrations of sulphur at which the band gap narrowing is minimum. Moreover, it would be difficult to incorporate sulphur into the TiO_2 crystal because of its large ionic radius (1.70 Å) compared to nitrogen (1.32 Å).

Recent experiments by Wang and Lewis, 2005, showed two optical absorption thresholds in TiO_2 samples corresponding to substitutional carbon dopants estimated at 5% atomic concentration. They also obtained increased efficiency in splitting water, which was higher than the efficiency observed at 0.32% carbon concentration. This confirms that there is an optimal dopant concentration for an optimum photoreactivity of C–doped TiO_2. In their theoretical investigation supported by experimental evidence, they concluded that both band gap narrowing and overlap between the oxygen 2p and dopant states induced by carbon strongly affects the photoreactivity of TiO_2. Hence higher C–doping concentration leads to more efficient photoactive reactions of TiO_2. However, the understanding of the exact mechanisms on how carbon–doping influences the electronic structures of TiO_2 so that it absorbs in the visible–light region at these concentrations is still rather limited.

Fluorine doping in TiO_2 had been carried out by gas–phase HF treatment at high temperatures, sol–gel techniques and ion implantation. The photo–response performance of F–doped TiO_2 was found to be enhanced due to reduction of the recombination rate of the photo–generated charge carriers (Hatori et al, 1998). An improved film densification and crystallinity caused by fluorine doping was observed by Ayllon et al, 2000, and Todorova et al, 2007. Nonetheless, the F–doped TiO_2 films indicated that most of absorption was still centred within the ultra–violet light region.

Various studies by Wang et al, 1994; Umebayasi et al, 2003b; Ruiz et al, 2003, and Anukunprasert et al, 2005 on niobium doping in TiO_2 have been focused on optimizing the visible light absorption of TiO_2 for a wide range of applications. A number of fabrication techniques (such as sputtering, high temperature diffusion, ion

implantation, sol–gel etc) with varying niobium concentrations (mmol or mol % Nb) have been attempted. However, due to low visible light absorption efficiencies of the Nb–doped TiO_2 obtained in these studies, the practicability and commercial viability of the fabricated photoelectrode films are still far from being achieved. In an effort to study and explore the possibilities of improving the visble light absorption capacity of Nb–doped TiO_2 prepared by high temperature diffusion, we focus mainly on the effect of concentration (at mmol %) of the niobium dopant states on the optical and structural characteristics of TiO_2.

CHAPTER THREE
THEORY

3.1 Introduction

In this chapter, the theory of Nb-doping in TiO_2 lattice is discussed and various aspects of their photochemical response analyzed. The chapter ends with the presentation of optical characteristics and determination of optical band gap of colloidal thin films.

3.2 Effects of Nb–doping into TiO_2

TiO_2 (anatase and rutile) have tetragonal structures (Fig. 3.1) with the bonding type in solid being intermediate between ionic and covalent at room temperature.

(a)Anatase TiO_2 crystal (b) Rutile TiO_2 crystal
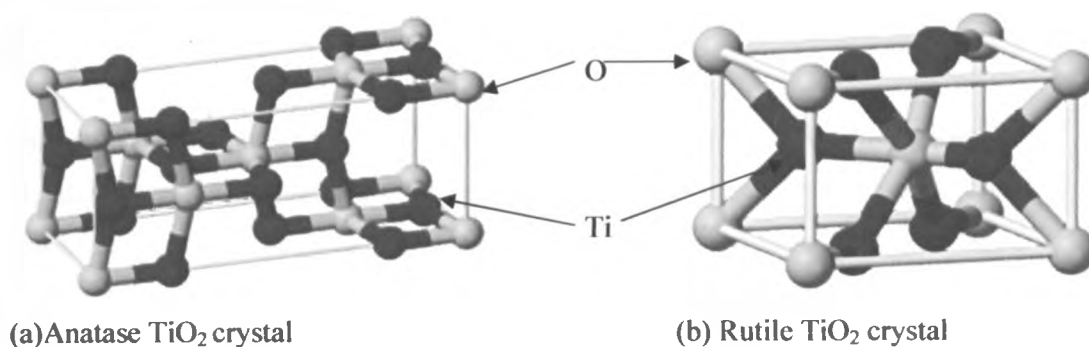
Fig. 3.1: 3–D crystal structure of rutile and anatase TiO_2: Grey balls represent oxygen atoms while the red balls stand for titanium atoms (source:*http://en.wikipedia.org/wiki/Titanium-dioxide*)

Ti has an electron configuration of (Ar) $3d^2$ $4s^2$ as shown in Fig.3.2. This means that in its stable state, its atom has the inert argon atomic structure followed by four electrons in its outermost energy level split into $3d^2$ and $4s^2$ orbitals. Hence, Ti has a valency of four.

Ti^{4+} has a $3d^0$ electron configuration, i.e., no electrons in the 3d level. This is reflected in the band structure where the conduction band has predominantly Ti3d character and the valence band predominantly O2p character (Umebayashi *et al*, 2003b).

$$2 \quad : \quad 8 \quad : \quad 8 \quad : \quad 3d^2 \quad : \quad 4s^2$$
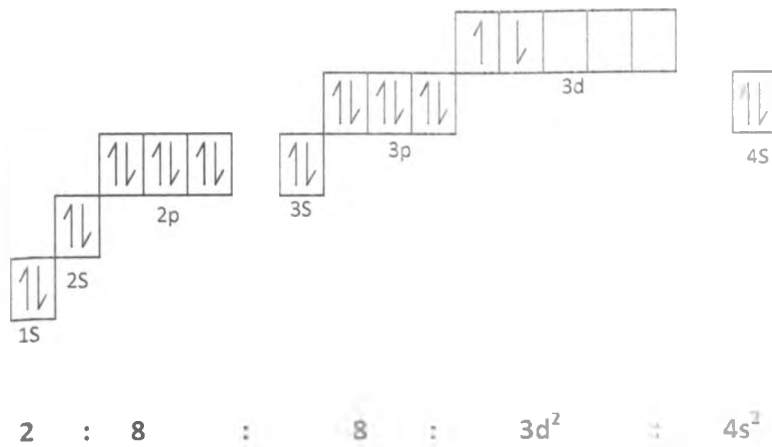
Fig. 3.2: Electron configuration of Ti atom showing number of electron in their orbitals at various energy levels: lower energy orbitals are filled before higher energy orbitals. Spin up–spin down of electrons are also shown (Source: Banergee *et al*, 2002)

Nb has an electron configuration of (Kr) $4d^5 \, 5s^2$ as shown in Fig. 3.3. This means that in its stable state, its atom has the inert krypton atomic structure followed by five electrons in its outermost energy level split into $4d^5$ and $5s^2$ orbitals. Hence, Nb has a valency of five.

Nb^{5+} has a $5s^0$, $4d^0$ electron configuration, i.e., no electrons in the 5s and 4d levels. Its conduction band structure in Nb_2O_5 has predominantly Nb4d character and the valence band predominantly O2p character. The ionic radius of Ti^+ is 0.64 Å while that of Nb^{5+} is 0.69 Å (Wang *et al*, 1994). It can be noted that Nb^{5+} ions have lost one additional valence electron compared to Ti^{4+} and are therefore expected to act as electron donors in TiO_2 (Miyagi *et al*, 2004).

2 : 8 : 18 : 8 : $4d^3$: $5s^2$
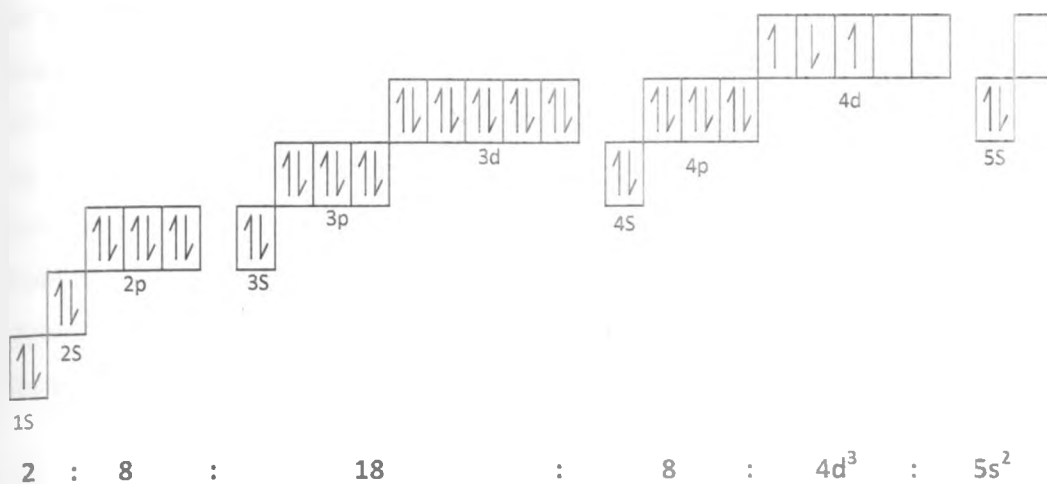
Fig. 3.3: Electron configuration of Nb atom showing number of electrons in their orbitals at various energy levels: lower energy orbitals are filled and their electrons paired before higher energy orbitals. Spin up–spin down of electrons are also shown (Source: Banergee *et al*, 2002)

Borgarelo *et al*, 1982, observed an increased rate of water cleavage (hence photoreactivity) under visible light upon introducing niobium cations (Nb^{5+}) into the TiO_2 lattice using Ru (bipy)$_3^{2+}$ as a sensitizer. They further reported that anatase TiO_2 doped with 0.4% Nb_2O_5 and loaded with 7.5 % Pt. and 0.1% RuO_2 exhibited optimal photoreactivity. These observations led to the suggestion that incorporation of cations of valence higher than that of the parent cation (e.g., Nb^{5+}) into the crystal matrix of TiO_2 results in enhanced photoresponse into the visible light region. Niobium doping in TiO_2 has been studied for many years. It can dissolve in TiO_2 isotropically to form solid solutions with TiO_2 in a wide concentration range (Choi *etal*, 1994). Wang *et al* 1994 noted that niobium seemed to be an optimum dopant choice into TiO_2 because it is pentavalent (Nb^{5+}) and has a comparable ionic radius (0.69Å) to that of Ti^{4+} (0.64) in TiO_2. But Choi *et al*, 1994 further reported that Nb^{4+}/Nb^{5+} energy levels lie close to Ti^{3+}/Ti^{4+} energy level. Because of this proximity of the charges, the trapped electron in Nb^{4+} can easily be transferred to a neighbouring surficial Ti^{4+} which leads to interfacial electron transfer. This makes the niobium dopant in TiO_2 colloids to function as an interfacial charge transfer mediator thereby increasing its photo–response.

Feroni *et al*, 2000 also observed Nb^{5+} substitution on Ti^{4+} lattice sites, and attributed the increase in the film's conductance of Nb–doped TiO_2 to dopant ionization or creation of an equal amount of Ti^{3+} ions in the TiO_2 lattice in order to compensate for substitution. Since the ionic radius of Nb^{5+} is similar to Ti^{4+}, it is therefore expected that niobium acts as donor atom when dissolved in TiO_2 because of charge transfer from the Nb 5s derived states to the TiO_2 conduction band (Andreas *et al*, 2006). Niobium therefore affects the electrical properties of Nb–doped TiO_2 as a donor–dopant by reducing the film's resistance. Hence, Nb–doped TiO_2 films exhibit high electron conductivity.

Findings by Umebayasi *et al*, 2003b, from the density of states (DOS) and electron density maps (EDMS) for Nb–doped TiO_2 prepared by ion implantation gave a photoelectron peak due niobium impurity at an electron–occupied level close to the bottom of the upper orbital (t_{2g}) of Ti3d conduction band (CB). This showed that the mid–gap levels of Nb–doped TiO_2 consist of the electronic states delocalized over the Ti_{t2g} and Nb_{t2g} orbitals. Hence the impurity level of Nb is close to the TiO_2 conduction band (CB). This result in an overlap of these levels and therefore optical excitation easily occurs from the valence band (VB) into the Nb impurity band tail and a thermal transition exists between the impurity level and the TiO_2 conduction band (CB). This results in a red shift of the optical absorption edge.

3.3 Effect of Concentration of Niobium on the Optical and Structural Characteristics of Nb–doped TiO_2

Low Nb^{5+} ion doping (mmol%) in TiO_2 is preferred for especially for solar cell and gas sensing thin film photoelectrode applications. This is because for these applications, a larger percentage in anatase Nb–doped TiO_2 is required and various studies have found that trace Nb–doping retard anatase–rutile phase transformation process even at high doping temperatures (> 800 °C) (Arbiol *et al*, 2002; Karvinen, 2003; Scotter *et al*, 2005). Low Nb–doped TiO_2 films posses excellent short and long range structural order with very high crystalline quality (Thevuthasan *et al*, 1996). Such trace Nb–doped TiO_2 films are less light scattering and also produce electronic structures in the TiO_2 crystal which are less distorted.

Electrodes with lower (trace) Nb–doping concentration (mmol %) were found to yield higher photocurrent densities than those with higher Nb–doping concentrations (mol %) (Wang *et al*, 1994). They obtained two optimal photoresponses at 0.03 at. % (for mmol % 0.02 at.% – 0.06 at. %)and 0.6 at.% (for mol % 0.2 at. % – 0.6 at. %) niobium concentrations in TiO_2 matrix representing a shift into the visible light absorption of 429 nm and 423 nm respectively. Higher Nb–doping is therefore relatively less photoactive because of enhanced electron–hole pair recombination rate which may be attributed to Nb=O clusters, cation vacancy formation, $TiNb_2O_7$ traces, surface states, cation coordination and bonding of intermediate reaction products.

Feroni *et al*, and Madare *et al*, 2000, obtained a considerable reduction in anatase–rutile phase transformations due to 5.00 at. % and 0.35 at.% Nb–doping respectively at a calcination temperature of 850 °C. They also reported a resultant average grain size below 40 nm. Nevertheless, TEM analysis of their results revealed considerable rutile phases in the Nb–doped TiO_2 films. Recent studies by Anukunprasert *et al*, 2005 observed optimal photoreactivity at 3 at.% Nb–doping calcined at 850 °C. Although they reported an inhibition of anatase–rutile phase transformatiom at this dopant concentration, their XRD results indicated a remarkable percentage of rutilization with subsequent grain coarsening. At a relatively lower doping temperature of 800 °C, Riuz *et al*, 2003 obtained suppressed photoreactivity at 4 at.% Nb–doping in TiO_2.

The amount of Nb–doping in TiO_2 affects both refractive index and transmittance of the Nb–doped TiO_2 films. Since Nb–doping in TiO_2 inhibits anatase–rutile phase transformation, this leads to an increase of the weight percentage of anatase phase. Hence the Nb–doped TiO_2 films exhibit lower refractive index and a higher transmittance compared to the undoped TiO_2.

3.4 Effects of Calcination on Microstrutural and Optical Characteristics of Nb–doped TiO_2

At higher calcination temperature (> 600 °C) the undesirable anatase–to–rutile TiO_2 phase transformation becomes a very fast process (Porter *et al*, 1999). At the same time, very high temperatures, (> 1150 °C) are required for appreciable Nb–doping into

TiO$_2$ lattice to take place, while ensuring enough thermal stability in Nb–doped TiO$_2$ (Niishiro *et al*, 2005).

Minero *et al*, 1989, and Sclafani *et al*, 1990, in their studies on variation of surface area and porosity of TiO$_2$ with calcinations, observed that pore narrowing is caused by a marked increase in grain size, thereby resulting in a marked decrease in both surface area and pore volume. Edelson and Glaezer, 1988, and Hague and Mayo, 1993, proposed that intra–agglomerate densification and grain growth occur relatively rapidly compared to interagglomerate densifiction. The observation that rutile crystallites grow much rapidly than anatase at high temperatures (above 600 °C) suggests that the relative order of the rates of the three process would be, intra–agglomerate densification > anatase–to–rutile transformation> interagglomerate densification.

In order to reduce the inactive rutile content in Nb–doped TiO$_2$ during calcinations, it can be calcined at temperatures between 600 to 900 °C for a variable period of time (Karakitsou and Verykios 1993). Most Nb–doped TiO$_2$ films annealed at 850 °C feature grain size below 40 nm, as only a fraction of anatase phase had been converted to rutile. This is because Nb–doping had been found to be a good anatase–to–rutile phase transformation inhibiter and hinders grain growth at considerably higher temperatures (800–900 °C) (Feroni *et al*, 2003; Madare *et al*, 1999; Ruiz *et al*, 2003; Anukunprasert *et al*, 2005; Karvinen, 2003). It is worth pointing out that although appreciable doping of niobium into the TiO$_2$ matrix is expected to have taken place at higher doping temperatures (> 1150 °C), with subsequent enhanced photoreactivity, segregation of niobium on the grain boundaries at such a high doping temperature cannot be ruled out. This may in turn increase electron–hole pair recombination rate of the Nb–doped TiO$_2$ (Wang *et al*, 1994). It is therefore imperative to choose a compromise temperature which ensures that a higher percentage of the doped–TiO$_2$ remains in its anatase phase during Nb–doping.

3.5 Optical Characteristics of Nb–doped TiO$_2$.

3.5.1 Reflectance spectra of Nb–doped TiO$_2$

Nb–doped TiO$_2$ with a higher anatase percentage absorbs more efficiently in the visible region (400–650) than that with a higher rutile (lower anatase) percentage

(Karvinen, 2003b). From his result on diffuse reflectance spectra, it was noted that the reflectance spectra of Nb–doped TiO_2 with a higher anatase percentage showed an absorption onset at 413 nm while that of Nb–doped TiO_2 with a higher rutile percentage has an absorption onset at 383 nm. The shift in the reflectance spectra leads to the conclusion that Nb–doping introduce energy levels in the band gap of anatase TiO_2 that are responsible for the shift to the red of the intrinsic absorption edge of TiO_2 and for the enhancement of the visible light absorption.

Studies by Karakitsou and Verykios, 1993 obtained similar results from diffuse reflectance spectroscopy in the form of the function F(R) versus versus wavelength in the region 200–600 nm using a Nb–dopant concentration of 1 wt. % on an oxide basis (where F(R) is the ratio of absorption scattering coefficient in the Kubelka–Munk equation and R is the optical reflectance), given by:

$$F(R) = \frac{(1-R)^2}{2R}$$ .... (3.1)

3.5.2 Transmittance spectra of Nb–doped TiO_2 on glass substrate

Niobium addition into the TiO_2 lattice suppresses the driving force for anatase–rutlie phase transformation at relatively high doping temperatures (> 850 °C). Because of this, Nb–doped TiO_2 exhibits a relatively higher transmittance than the undoped TiO_2. Therefore, the Nb–doped TiO_2 with subsequent higher percentage anatase structures results in films with both lower density and refractive index (Mardare et al, 2000). This may mean that a more porous film surface is induced by Nb–dpoing.

3.5.3 Optical absorption of colloidal semi-conductor particles

An important technique of measuring the band gap energy of a semiconductor is the absorption of incident photons by the material. Here photons of selected wavelengths are directed at the sample, and relative transmission of the various photons is observed. Since photons with energies greater than the band gap energy are absorbed while photons with energies less than the band gap are transmitted, a fairly accurate measure of the band gap energy can be obtained.

It is apparent from figure 3.4 that a photon with energy $h\nu \geq E_g$ can be absorbed in a semiconductor. Since the valence band contains many electrons and the conduction band has many empty states into which electrons may be excited, the probability of photon absorption is high. As figure 3.4 indicates, an electron excited to the conduction band by optical absorption may initially have more energy than is common for conduction band electrons (almost all electrons are near E_g unless the samples are heavily doped). Thus the excited electron loses energy to the lattice in scattering events until its velocity reaches the thermal equilibrium velocity of other conduction band electrons (Banerjee *et al*, 2002). The electron and hole created by this absorption process are excess carriers since they are out of balance with their environment, they must eventually recombine. While the excess carriers exist in their respective bands, however, they are free to contribute to the conductivity of the material.
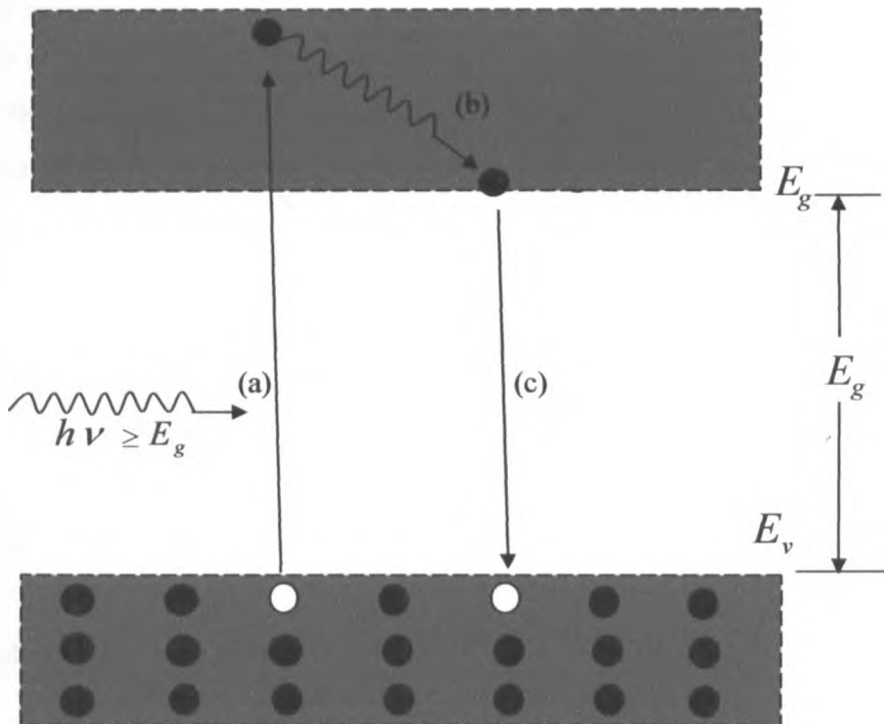
Fig 3.4: Optical absorption of a photon with $h\nu \geq E_g$: (a) an electron–hole pair is created during photon absorption; (b) the excited electron gives up energy to the lattice by scattering events; (c) the electron recombines with a hole in the valence band (Source: Banergee *et al*, 2002)

A photon with energy less than E_g is unable to excite an electron from the valence band to the conduction band. Thus in a pure semiconductor, there is negligible absorption of photons with $h\nu < E_g$. This explains why some materials are transparent in certain wavelength ranges. We are able to "see through" certain insulators, such as good NaCl crystal, because a large energy gap containing no electron states exist in the material. If the band gap is about 2 eV wide only long wavelengths (infrared) and the red part of the visible spectrum are transmitted; on the other hand, a band gap of about 3 eV allows infrared and the entire visible spectrum to be transmitted.

If a beam of photons with $h\nu > E_g$ falls on a semiconductor, there will be some predictable amount of absorption, determined by the properties of the material. We would expect the ratio of transmitted to incident light intensity to depend on the photon wavelength and the thickness of the sample. To calculate this dependence, it can be assumed that a photon beam of intensity I (photons/cm^{-2}s) is directed at a sample of thickness t, and the beam contains only photons of wavelength λ, selected by a monochromator. As the beam passes through the sample, its intensity at a distance λ from the surface can be calculated by considering the probability of absorption within any increment dx. Since a photon which has survived to x without absorption has no memory of how far it has traveled, its probability of absorption in any dx is constant. Thus the degradation of the intensity $-dI(x)/dx$ is proportional to the intensity remaining at x

$$-\frac{dI(x)}{dx} = \alpha I(x) \dotfill (3.2)$$

The solution to this equation is

$$I(x) = I_o e^{-\alpha x} \dotfill (3.3)$$

The coefficient α is called the absorption coefficient and has units of cm^{-1}. This coefficient will of course vary with the photon wavelength and with the material. If there is negligible absorption at long wavelengths ($h\nu$) and considerable absorption of

21

photons with energies larger than E_g, the relation between photon energy and wavelength is $E = hc/\lambda$ and if E is given in electron-volts and λ in nanometers, this becomes $E = 1240/\lambda$

Optical absorption coefficient of semi-conductor films can be evaluated from transmittance using the relation

$$T = A \exp(-\alpha t) \quad \text{.. (3.4)}$$

where: A = coefficient related to refractive index and is nearly equal to unity at the absorption edges, α = absorption coefficient, t = film thickness, T = transmittance.

Semiconductors absorb light below a threshold wavelength λ_g, and the fundamental absorption edge is related to the band gap energy via the relation:

$$E_g = \frac{1240}{\lambda_g} \quad \text{.. (3.5)}$$

where E_g = band gap, λ_g = threshold wavelength.

However, within the semiconductor, the light extinction follows Lambert–Beer's Law:

$$I = I_0 e^{-\alpha l} \quad \text{.. (3.6)}$$

where: l = penetration depth of light.

Near the threshold, the band gap energy (E_g) of the film is estimated from the absorption coefficient using the relation

$$\alpha h\nu = E(h\nu - E_g)^n \quad \text{.. (3.7)}$$

where: B = Edge width parameter, $h\nu$ = incident photon energy, n = exponent that determines the type of electronic transition causing absorption which is $\frac{1}{2}, \frac{3}{2}, 2, 3$ for direct allowed, direct forbidden, indirect allowed, and indirect forbidden transitions respectively (Madare *et al*, 2000).

A direct allowed transition is one in which a plot of the electronic energy against the wave vector, the minimum of the conduction band states is placed vertically above the maximum of the valence band energy states. For an indirect allowed transition, the two extremes are displaced from each other, and so the threshold excitation requires a contribution of lattice phonons so as to compensate for the change in the wave vector. This in turn reduces the absorption cross-section and hence the value of α. Nb–doped TiO_2 belongs to the indirect allowed transition semiconductors (Mardare *et al*, 2000) and so the value of n is equal to 2.

The reflectivity $R_{(\lambda)}$ at any absorbing medium of indices (n, k) in air for normal incidence is given by:

$$R_{(\lambda)} = \frac{(1-n)^2 + k^2}{(1+n)^2 + k^2} \quad \dots\dots\dots\dots\dots\dots\dots\dots\dots\dots\dots\dots\dots\dots\dots\dots\dots (3.8)$$

In the visible region, the absorption coefficient α is influenced by the scattering of light on the surface roughness (if light scattering dominates over the absorption), the transmission coefficient $T_{(\lambda)}$ can be obtained from the relation:-

$$T = \frac{(1-R)^2 + \exp(-\alpha(\lambda)t)}{1 - R^2 + \exp(-2\alpha(\lambda)t)} \quad \dots\dots\dots\dots\dots\dots\dots\dots\dots\dots\dots\dots\dots\dots (3.9)$$

where: R = Reflectance, T = transmittance, t = thickness of the film, λ = wavelength

3.5.6 Optical band gap

At shorter wavelengths, close to the optical band gap, the scattering losses are dominated by fundamental absorption and relation (3.4) is often used (Mardare *et al*,

2000). Above the threshold of the fundamental absorption, the dependence of α on incident energy is given by the equation (3.7).

For a more detailed analysis of the spectral absorption characteristics, we use the relation:

$$\alpha(E) \propto \left[1 - \frac{2}{\pi} tan^{-1}\left(\frac{E_g - E}{\Sigma}\right)\right] \dots\dots\dots\dots\dots\dots\dots\dots\dots\dots\dots (3.10)$$

where: Σ = energy spread of the electronic transitions giving rise to the band gap (Rodriguez *et al*, 2000). Taking into consideration the Urbach tail of the absorption characteristics, relation (3.10) above becomes:

$$\alpha(E) \propto exp\left[\frac{E - E_\phi}{\Delta E}\right] \dots\dots\dots\dots\dots\dots\dots\dots\dots\dots\dots\dots\dots (3.11)$$

where: ΔE = parameter representing the width or slope of the exponential tail, E_ϕ = a constant characteristic of the film material.

3.5.7 Determination of optical band gap energies of the prepared Nb–doped TiO$_2$ films using optical transmittance data.

Consider a semiconductor with thickness t (Fig. 3.5) and an absorption coefficient that is given by:

$$\alpha(E) \propto \sqrt{E - E_g} \dots\dots\dots\dots\dots\dots\dots\dots\dots\dots\dots\dots\dots\dots\dots (3.12)$$
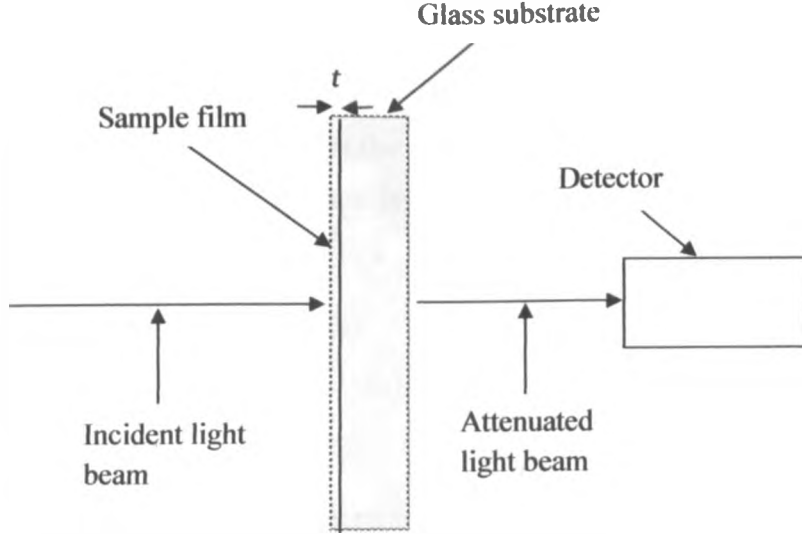
Fig. 3.5: An illustration of the optical spectroscopy for optical band gap determination of the Nb–doped TiO_2 films.

Light incident on the semiconductor material will be partially reflected due to Fresnel reflection with Fresnel power reflection coefficient (R_1) being given by:

$$R_1 = \left(\frac{n_s - 1}{n_s + 1} \right)^2 \dotfill (3.13)$$

where n_s is the refractive index of the film.

Assuming that the intensity of the light incident on the semiconductor is I_o, the light intensity just inside the semiconductor (I_{s1}), is given by

$$I_{s1} = I_o(1 - R_1) . \dotfill (3.14)$$

Thus the light intensity at the lower end of the semiconductor layer (I_{s2}) is given by

$$I_{s2} = I_o(1 - R_1)\exp(-\alpha t) \dotfill (3.15)$$

Further, consider Fresnel reflection at the semiconductor–substrate and substrate-air interfaces and denote them by R_2 and R_3. Furthermore, if the substrate surface is not polished (i.e., has a surface roughness), there will be optical scattering losses. Assuming that the fraction of light that does not reach the detector due to scattering at the un–polished substrate surface is S, then the measured optical transmittance through the material is given by:

polished (i.e., has a surface roughness), there will be optical scattering losses. Assuming that the fraction of light that does not reach the detector due to scattering at the un–polished substrate surface is S, then the measured optical transmittance through the material is given by:

$$T(E) = \frac{I_{transmitted}}{I_o} = (1 - R_1)(1 - R_2)(1 - R_3)(1 - S)\exp(-\alpha t) \quad \text{................................} \quad (3.16)$$

where we have neglected interference effects and multiple reflections. Solving equation (3.16) above for the absorption constant $\alpha(E)$ yields

$$\alpha(E) = -\frac{1}{t}\ln\left(\frac{T(E)}{(1 - R_1)(1 - R_2)(1 - R_3)(1 - S)}\right) \quad \text{...........................} \quad (3.17)$$

Normalizing the transmittance data so that $T_{normalized}(E) \leq 100\%$ in the transparent region ($hv < E_g$), allows us to neglect Fresnel reflections and scattering losses. We then write

$$\alpha(E) = -\frac{1}{t}\ln(T_{normalized}(E)) \quad \text{..} \quad (3.18)$$

But according to equation (3.12), $\alpha(E)$ has square–root dependence on E. Accordingly, $\alpha(E)^2$ has a linear dependence on E.

CHAPTER FOUR
EXPERIMENTAL TECHNIQUES

4.1 Introduction

In this chapter, the experimental techniques used in Nb–doping of TiO_2 and the fabrication of Nb–doped TiO_2 thin films of niobium concentration range of 0.02–0.06 at. % are discussed. The chapter ends with how the optical characteristics, crystal structure and composition of the Nb–doped TiO_2 were determined.

In our study, high temperature diffusion was employed to synthesize the Nb–doped TiO_2. This technique involves mixing high purity powders of TiO_2 and Nb_2O_5 in various molar ratios and then firing in air for various periods of times. A similar method was used by Karakitsou and Verykios, 1993; Wang *et al*, 1994; Radecka and Rekas, 1995; Niishiro *et al*, 2005.

4.2 Preparation of Nb–doped TiO_2

To obtain the desired Nb^{5+} concentration in the TiO_2 matrix, calculated masses (Appendix I) of Nb_2O_5 (99.9% purity, Aldrich from Germany) were weighed and mixed with 10.000 g of TiO_2 (Degussa P–25) using a digital electric balance of accuracy $\pm$ 0.005 cm^3. Distilled water (50.00 cm^3) was then added to the mixtures in 100 cm^3 beakers (Table 4.1).

Table 4.1: Calculated niobium doping concentrations in TiO_2

Sample No.	Mass of Nb_2O_5 $\pm$ 0.005 (g)	Mass of Nb_2O_5 (g)+ TiO_2 $\pm$ 0.005 (g)	Mole % Nb^{5+} in TiO_2	At.% Nb^{5+}	Amount of distilled water used = 0.01(cm^3)
1	0.010	10.010	0.1197	0.02	50.00
2	0.015	10.015	0.1796	0.03	50.00
3	0.020	10.020	0.2394	0.04	50.00
4	0.030	10.030	0.3591	0.06	50.00

The slurry was gently heated to 80 °C under continuous stirring (using a magnetic stirrer) until nearly all the water evaporated. The rate of stirring was reduced after every one hour to avoid spilling of the slurry. The solid residue was further dried in a furnace at 110 °C for about 10 hours. Using a mortar and pestle, the solid was crushed

into fine powder then sieved using a sieve of 106 μm pore size. The samples were then placed into fused silica glass boats and calcined (heat treated) in a furnace (Nabertherm–30) (Fig. 4.1) fitted with a programme controller C 30 at a temperature of 850 °C for 5 hours to achieve appreciable doping. The calcination temperature was approached at a heating rate of 1.5 °C /min or 0.025 °C/sec.

Fig. 4.1: Photograph of Nabertherm–30 furnace

4.3 Preparation of Nb–doped TiO₂ Colloidal Solution

A paste of 0.371g of Nb–doped TiO_2 was mixed with the same mass of de–ionized water. The mixture was then ground for 10 hours using an agate mortar (Fig. 4.2). The paste was then diluted with w:w triton water (Triton X–100 Aldrich) solution to 36% w:w with respect to the Nb–doped TiO_2. A few drops of 0.5M nitric acid were added to facilitate the dispersion of the Nb–doped TiO_2 particles and reduce their agglomeration. The resulting gels were then stirred with a magnetic stirrer overnight and were then stored under refrigeration (at < 5 °C). Three colloidal solutions of Nb–doped TiO_2 were prepared for each Nb–doping concentration.
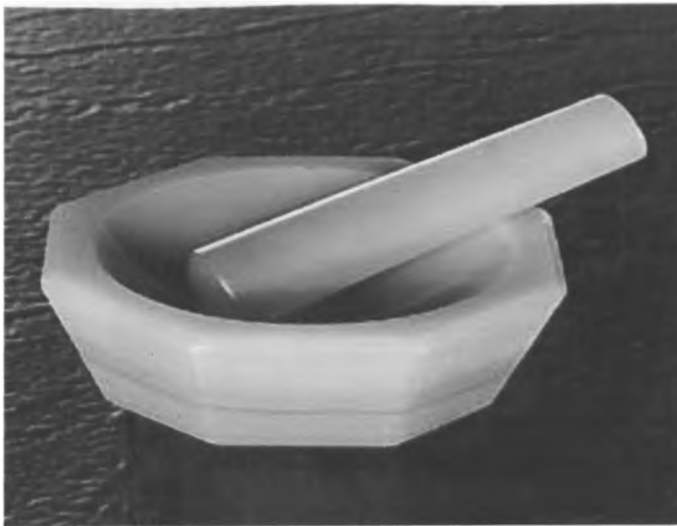
Fig. 4.2: Photograph of an Agate mortar and a pestle.

4.4 Thin Film Preparation

4.4.1 Cleaning of the glass substrates

Pieces of glass substrates (glass slides) were cut into 2 cm x 2 cm using a glass cutter. They were then cleaned using a mixture of aqueous sodium hydroxide ($NaOH_{aq}$) and liquid detergent (which had been prepared by mixing the two in the ratio of 1:3 respectively) by gently scrubbing them with cotton bud and finally drag–wiping with lens cleaning tissue. The surfaces were then cleaned gently using lens cleaning tissue wetted with isopropyl alcohol. This procedure was then repeated using acetone. The substrates were finally rinsed with deionized water in an ultrasonic cleaner for 30 to 35 minutes in order to remove any trace of dirt by agitating them out at ultrasound frequency. Using a twitter which had been rinsed with isopropyl alcohol and acetone, the substrates were removed from the ultrasonic cleaner and then dried by blowing hot air over them for about 10 minutes using a heat gun.

4.4.2 Thin film preparation using spin coating technique.

Using a dropper, a blob of Nb–doped TiO_2 colloidal solution was drawn and put at the centre of a cleaned glass substrate which had been centrally anchored on the spin–coater (P67080, Cookson Electronics–USA) turntable. The turntable cover was immediately replaced (this was done in order to avoid the drying of the blob). The spin speed (revolutions per minute) was adjusted at 2000 rev/min.and the spin–coater switched on. This was repeated several times for each Nb–doped TiO_2 sample

29

concentrations and the un–doped TiO_2 samples until three uniformed surface films were obtained for each. A total of fifteen films were prepared.

Fig. 4.3: Photograph of a spin coater P67080

The films were then heat treated (annealed) at a temperature of 450 °C using the Nabertherm–30 furnace at a heating rate of 1.5 °C/min. for 5 hours then cooled slowly at a rate of 0.3 °C/min. for 25 hours. The annealing was done in order to eliminate mechanical stress within the films and get rid of other organic material additives used in the preparation of the colloidal solutions.

NB: Before any coating on glass substrate was done, the colloidal solutions were stirred with a magnetic stirrer at 750 r.p.m for about 2 hours to ensure their uniformity.

4.5 Surface Profilometry and Thickness Measurements

The above measurements were done using an Alpha–Step–IQ thickness monitor interfaced with a microcomputer. Five different thickness measurements at different areas on the film surfaces were taken for each Nb–doped TiO_2 concentrations and the un–doped TiO_2 films. The final thickness of each sample was the mean of the thicknesses from the five areas of the test samples for each Nb–doped and the un–doped TiO_2 films.
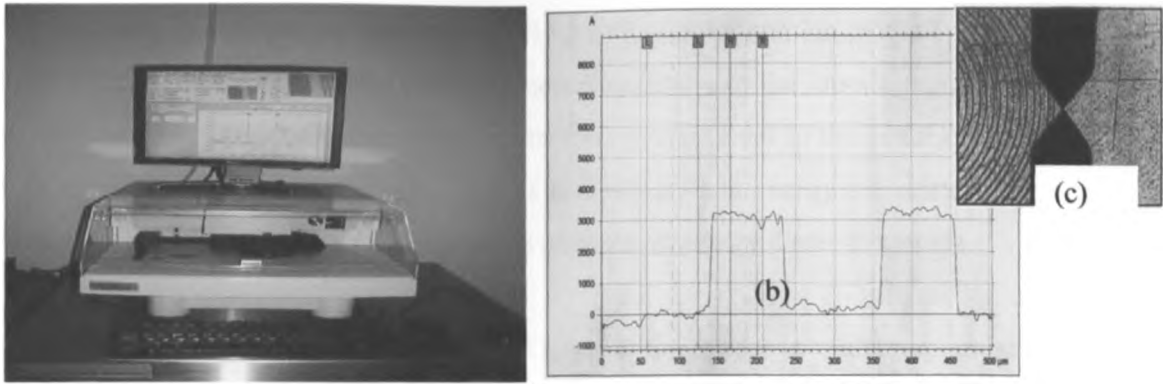
Fig. 4.4: (a) A photograph of an Alpha–Step IQ thickness monitor interfaced with a microcomputer (b) characteristic thickness spectrum showing movement of cursor positions (c) image of stylus movement across the film.

4.6 EDX.RF Measurements

To confirm the niobium doping in TiO_2 and their respective concentrations in the prepared samples, an EDX.RF spectrometer (CANBERRA Industries INC. USA) fitted with a SiLi detector that had a resolution of 210 eV at the Mn line was used (Fig.4.5).
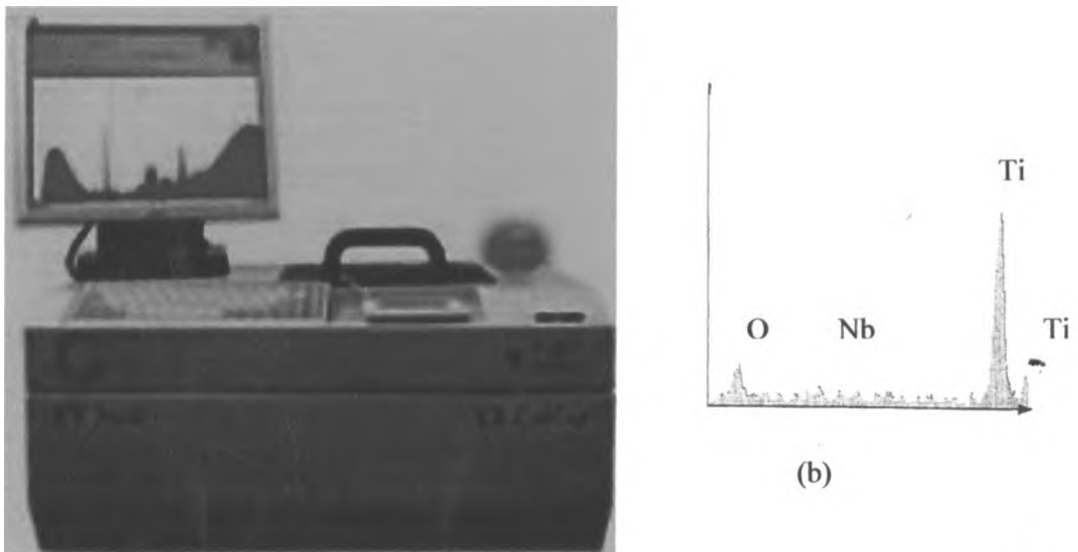
(a)

Fig. 4.5: (a) Photograph of an EDX.RF spectrometer SL 80175 interfaced with a microcomputer (b) characteristic EDX.RF spectrum.

The EDX.RF is based on Moseley's law (i.e., the square root of the frequencies of lines in atomic X-ray spectra depends linearly on the atomic number of the emitting atom) which relates "characteristic" fluorescence radiation to the atomic number of the emitting atom, and the fluorescence intensity is proportional to the concentration of an element present in the sample. Also as wavelength and energy are related, the fluorescence radiation can be evaluated in wavelength or energy dispersive mode.

A sample of the prepared Nb–doped TiO_2 was put under a radiation source (Cadmium–109) and analyzed by the X–Ray Spectrometer which consists of solid–state detector SiLi, pre–amplifier and a multi–channel analyzer (MCA). A microcomputer with a relevant interface was also incorporated (see Fig. 4.6). The pre–set live counting time for spectra collection was 33 minutes and 20 seconds for all the samples. The resultant spectra were collected on the multi–channel analyzer in the pulse height analysis mode. The reported final concentration of each element was the mean of the concentrations of the element from three samples. A total of twelve Nb–doped samples were analyzed.
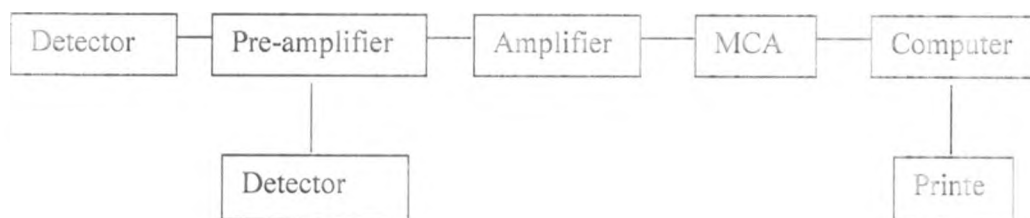
Fig.4.6: Block diagram of EDX.RF spectrometry.

4.7 X–ray diffraction (XRD) Analysis

These analyses were done using Siemens D–5000 (Theta/2Theta D 5000) powder diffractometer fitted with Cu Kα as the anode material.

(a)

(b)

Angle 2θ (degree)
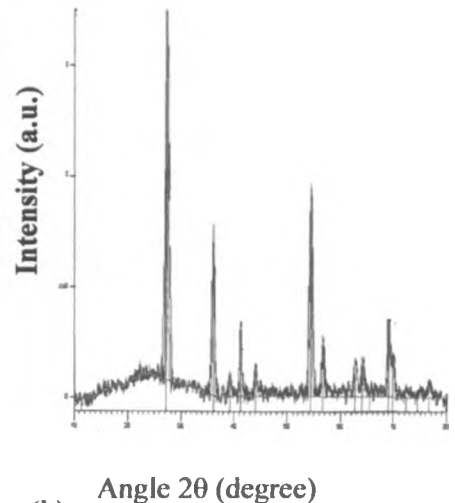
Fig.4.7: (a) Photograph of a Siemens D–5000 powder Difractometer (b) characteristic X–ray diffractogram.

The difractometer configurations were set at Start Position of 10.0000 and End Position of 80.0000 (^{o}2Th). An angle step size (^{o}2Th.) of 0.0200 and a scan step time (s) of 0.3000 seconds were used in a continuous scan type mode for all the samples. The generator settings were 45 kV and 40 mA. The raw data obtained for the angle positions (^{o}2Th.), height (ct/s), d–spacing (Å) and relative intensity (%) were used to draw the characteristic X–ray diffractograms of the samples using Origin–8 programme.

4.8 Optical Characterization

In order to obtain the optical properties the prepared films, the transmittance and reflectance spectra were analyzed using a Solid Spec–3700 DUV; UV–VIS–NIR Spectrophotometer (SHIMADZU-Japan). The reference spectrum for both transmission and reflection were obtained by using a clean uncoated glass substrate.

Fig. 4.8: (a) Solid Spec–3700 DUV; UV–VIS–NIR Spectrophotometer interfaced with a microcomputer.

After a pre–selection of the required function on the standard tool bar for emission, reflection, transmission, windows, the setting configurations of the spectrophotometer were selected. Using detector 2 for InGaAs and the photomultiplier (PMT), the desired spectral range was set at 250–1050 nm via the dialogue box. A reference sample of a clean glass slide of the same property as the substrate was then loaded into the spectrophotometer and run to obtain the reference spectral readings. This should give 100% straight line. The reference sample was then unloaded and replaced with the prepared Nb–doped electrode films under test. By using single measurement, a spectrum was displayed. The procedure above was repeated for all the prepared samples. The final spectrum of each sample was the mean of the spectra from three test samples for each Nb–doped TiO_2 films. It should be noted that noise and vibrations which may degrade the resolutions of the spectra should not be allowed in the vicinity of the equipment set–up.

4.9 Procedure for Obtaining Optical Band Gap from the Transmittance Data

The spectral transmittance was measured using the spectrophotometer (3700 Solid Spec. DUV measuring UV–VIS–NIR range) and the data converted to $T(E)$.

The $T(E)$ data was then normalized so that $T_{normalized}(E) \leq 100\%$ in the transparent region ($hv < E_g$) and the wavelengths were converted into energy E using the

34

relation $E = \dfrac{1240eV - nm}{\lambda}$. The normalized transmittance data was then plotted against energy E (Fig. 5.3).

The absorption coefficient $\alpha(E)$ was calculated using Eq. 3.18, and the square plots of $\alpha(E)^2$ versus E drawn with their linear fits made in the vicinity of the band-gap (Fig. 5.4). The intersections of linear fits with the abscissa were the band-gaps.

CHAPTER FIVE

RESULTS AND DISCUSSION

5.1 Introduction

In this chapter, the results of niobium doping in TiO_2, crystal structure of Nb–doped TiO_2 and optical characteristics of Nb–doped TiO_2 films with niobium concentrations of 0.02, 0.03, 0.04 and 0.06 at. % are discussed.

5.2 Effects of Calcination

The Nb_2O_5 / TiO_2 sample mixtures fired at 850 ^oC for five hours, turned from white to slightly yellow in colour. There was also noticeable volume shrinkage of the powder in the silica glass boats. The colour change may suggest that some appreciable doping had taken place and this agrees with previously reported results (Wang et al, 1994; Feroni et al, 2000; Ruiz et al, 2003; Scotter et al, 2005 and Andreas et al, 2006). The slight yellow colour may be attributed to polaron absorption due to niobium doping into the TiO_2 lattice. As the crystalline order increases, the absorption band becomes broader and shifts towards larger wavelength giving rise to the slight yellow colour (Schmitt and Aegerter, 2000).

5.3 EDX.RF Analysis

Figure 5.1 shows the EDX.RF results for the Nb–doped TiO_2 for 0.04 at. % Nb concentration.
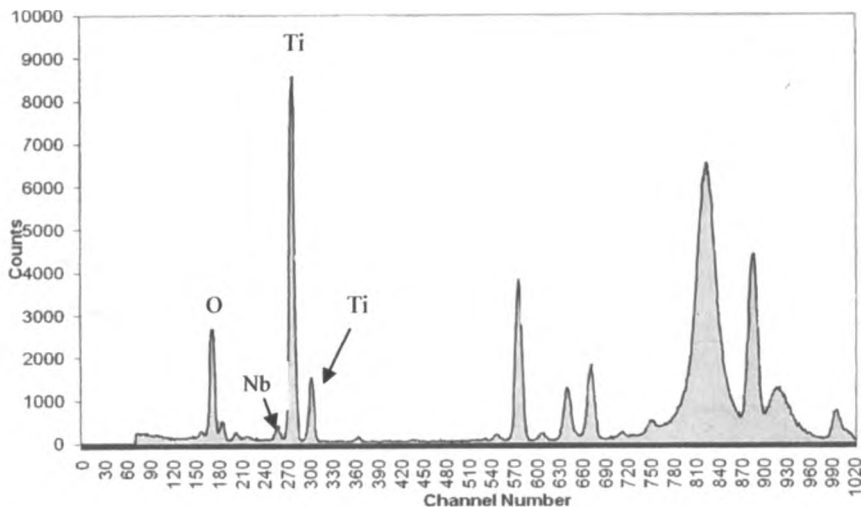

Fig. 5.1: EDX.RF spectra of Nb–doped TiO_2 (Nb concentration 0.04 at. %). The energy width of each channel is typically 1.33 eV/channel. The non–labelled spectra are due to interference phenomena.

The EDX.RF results confirm the chemical composition of the Nb–doped TiO_2 sample powders to contain Ti, Nb and O atoms. The non–labeled signals are called scatter peaks and are caused by noise and interference phenomena, i.e. coherent and incoherent pulses. They represent signals which arrive briefly one behind the other and cannot be differentiated by the spectroscopic amplifier despite being recognized by the fast channel, thereby resulting in inefficient pulse pile–up discrimination. The near similarity between ionic radii of Nb^{5-} (0.69 Å) and Ti^{4-} (0.64 Å) suggest substitution of Nb at Ti lattice sites at the doping concentration range (0.02–0.06 at. % Nb) used. However, at our doping temperature of 850 °C, existence of traces of impurity Nb_2O_5 and TiO_2 mixed powders, $TiNb_2O_7$, O–Nb=O, and effect of oxygen activity on niobium segregation may also contribute some significant effect on the resultant spectrum.

5.4 XRD Results

Figure 5.2 shows the XRD spectrum obtained from the Nb–doped TiO_2 samples. The results indicate a slight phase modification at 0.04 at. % Nb–doping concentration. It is seen from Table 5.1 that the sample with this niobium doping concentration also displayed the smallest average crystallite size (39.923 nm) and the highest anatase percentage (37 %). This suppression of exaggerated grain growth may be due to Nb^{5-} substituting for Ti^{4+} in the anatase crystalline lattice. Feroni *et al*, 2000 also noted a reduction in TiO_2 nanoparticle sizes due Nb addition in TiO_2 films calcined at 850 °C. They reported a nearly similar grain size of 40 nm with only a small fraction of anatase having been converted to rutile at this calcination temperature. Karviner, 2003, found that Nb–doping concentration of 0.067 at. % calcined at 860 °C for 1.5 hours accelerated anatase–rutile phase transformation (119 nm) while relatively lower Nb–doping concentrations of 0.0132 and 0.172 at. % calcined at the same temperature and time yielded crystal sizes of 37 and 39 nm respectively. Except for slight variations in calcinations temperatures and Nb–doping concentrations, our results therefore match closely with those in literature.
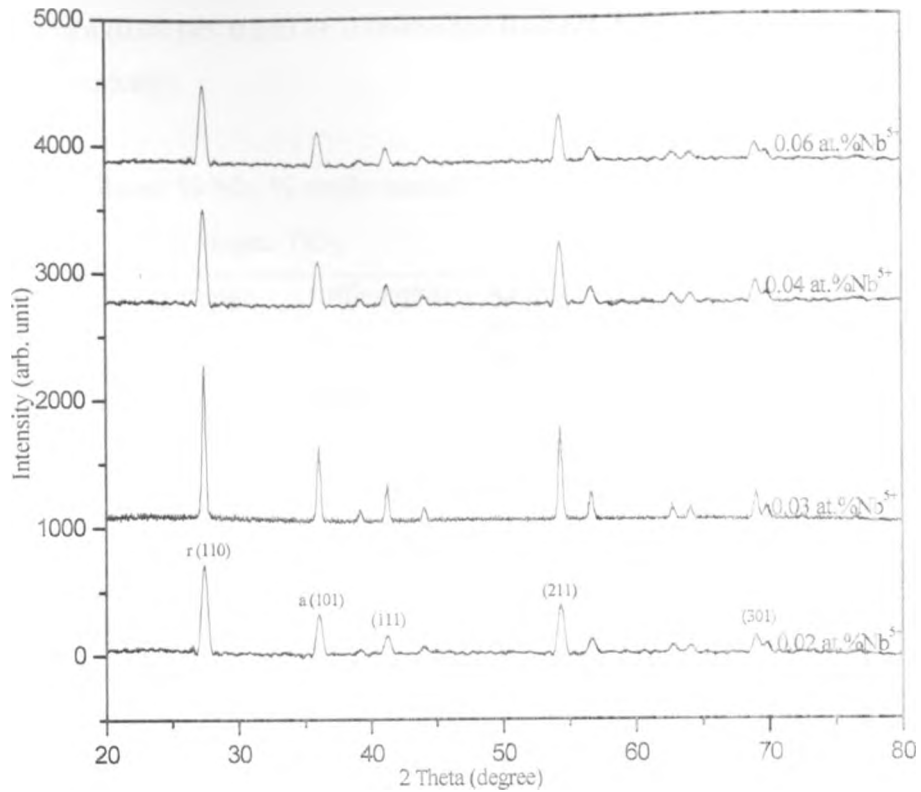
Fig.5.2: **XRD spectra** of Nb–doped TiO_2 for niobium concentrations of 0.02, 0.03, 0.04 and 0.06 at. % calcined at 850 °C (r, rutile phase; a, anatase phase)

The percentage anatase–rutile contents in the doped samples were calculated using the equation:

$$x = \left(1 + 0.8\frac{I_A}{I_R}\right)^{-1} \quad\quad \dots\dots\dots\dots\dots\dots\dots\dots\dots\dots\dots\dots \quad (5.1)$$

where x is the weight fraction of rutile in the doped powder, while I_A and I_R are the X-ray intensities of anatase and rutile peaks respectively (Ding *et al*, 1996). The average crystal sizes from the line broadening of corresponding X-ray diffraction peaks were estimated using the Scherrer's equation:

$$l = \frac{K.\lambda}{\beta.\cos\theta} \quad\quad \dots\dots\dots\dots\dots\dots\dots\dots\dots\dots\dots\dots\dots\dots \quad (5.2)$$

where l is the crystallite size, λ is the wavelength of the X-ray radiation (1.54 Å for the difractometer used), K is usually taken as 0.94, β is the line width at half maximum height (0.00395, 0.00379, 0.00410 and 0.00391 Å for 0.02, 0.03, 0.04, 0.06 at. % Nb^{5+} respectively).

Table 5.1: Calculated % Nb, % rutile–anatase phases, average crystallite sizes and film thickness of the Nb–doped TiO_2.

% Nb^{5+}	Percentage phases rutile/anatse		Average crystallite size (nm)	Film thickness (μm)
	r(%)	a (%)		
0.02	69	31	41.407	6.65
0.03	72	28	43.141	5.84
0.04	63	37	39.923	5.81
0.06	70	30	41.604	4.57
Un-doped	75	25	125.157	5.98

Table 5.1 shows the average grain/crystal size and niobium concentration. It is noticed that at the calcination temperature of 850 °C, there was insignificant grain coarsening of Nb–doped TiO_2 provided the doping levels were low (0.02–0.06 at. % Nb.) This observation indicated that niobium addition inhibited grain growth thereby maintaining a high surface area of the powder. The results also indicate a phase modification when TiO_2 was doped with more than 0.06 at. % Nb at the present Nb–doping range. This might be due to Nb^{5+} substituting for Ti^{4+} in the crystalline TiO_2 lattice thus either hindering or accelerating the anatase–to–rutile phase transformation. Similar observations had also been made by Anukunprasert et al, 2005.

It is worth pointing out that our trace Nb–doping range of 0.02–0.06 at. % may not remarkably suppress anatase–to–rutile phase transformation and grain growth at the doping temperature used (850 °C). This result is fairly consistent with that obtained by Ruiz et al, 2003. However, our crystallite sizes results calculated from XRD analysis indicated that Nb–doping prevented exaggerated grain growth at our calcinations temperature.

5.5 Optical Characterization

Figure 5.3 shows the reflectance and transmittance spectra (in the 250 nm–1050 nm wavelength range) for un–doped and Nb–doped TiO_2 films at concentrations of 0.02 at. %, 0.03 at.%, 0.04 at % and 0.06 at.% Nb^{5+}. The average optical transmittance of the film within the above wavelength range is < 60%. From the plots, the transmittance of the Nb–doped TiO_2 films decrease with increase in niobium concentration. This may suggest that at the investigated niobium concentration range of 0.02–0.06 at. % Nb^{5+}, increasing niobium concentration generally result in an increase in light scattering loses. The kink at wavelength $(\lambda) \approx 700$ nm in the spectrum may have been caused by the change–over in switching on between the InGaAs and PbS detector units. It is called the switching step in the optional direct detector unit of the spectrophotometer used.

It is noted in Fig. 5.3 that all the Nb–doped TiO_2 film samples had their absorptions shifted into the visible spectrum compared to the undoped TiO_2. A sharp absorption beginning at 412.2 nm (3.017 eV) was obtained and this may be attributed to the introduction of niobium dopant concentration (0.04 at. % Nb^{5+}) which was responsible for the red shift due to enhancement of the visible light absorption. The result matches closely with that of Saila Karvinen, 2003 who obtained a sharp absorption at 413 nm (3.00 eV) for 0.027 at. % Nb^{5+} in TiO_2 calcined at 860 °C. It is also seen that samples with niobium concentrations of at. % 0.02 and 0.04 Nb^{5+} had the lowest % transmittance (highest absorptance) while that with niobium concentration of 0.06 at. % Nb^{5+} had the highest transmittance and therefore relatively lower absorptance. The un–doped TiO_2 film showed a fairly low transmittance (~45 % for 5.98 μm film film thickness). Madare et al, 2000 obtained a higher transmittance (~90 % for 0.3 μm film thickness) for un–doped TiO_2 film.
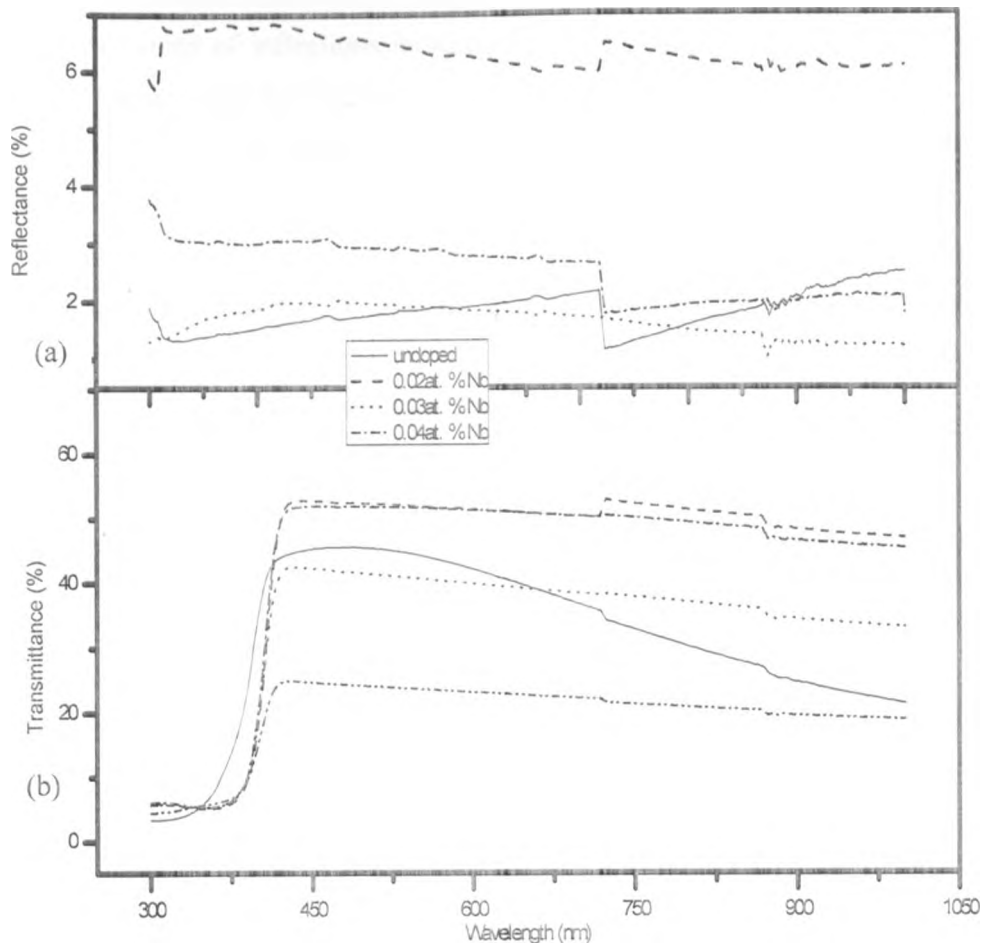
Fig. 5.3: (a) Reflectance spectra (%) and (b) Transmittance spectra (%) vs wavelength (nm) for 0.02, 0.03, 0.04 at. % Nb^{5+} and un–doped TiO_2. Reflectance spectrum for 0.06 at. % Nb^{5+} is omitted for clarity.

The films studied showed relatively very low reflectance less than 10 %. This is attributed to scattering loses caused by the surface roughness of the films. From the reflectance spectra, samples 0.02 at. % and 0.04 at. % Nb^{5+} concentration also had higher reflectance than the un-doped sample. Samples with 0.03 at.% and 0.06 at. % Nb^{5+} had coinciding but lower reflectance. Here again, the kink at wavelength (λ) $\approx$ 700 nm in the spectrum may have been caused by the InGaAs and PbS switching step in the optional detector unit of the spectrophotometer.

Figure 5.4 shows the normalized transmittance versus energy for the Nb–doped TiO$_2$ and un–doped TiO$_2$ films. From the normalized transmittance versus energy spectra, it is seen that the points of inflections indicating the onset of absorptions are shifted more towards lower energy for 0.02 and 0.04 at. % Nb^{5+} than 0.03 and 0.06 at.% Nb^{5+} doping as compared to the un–doped TiO$_2$. This observation further reinforces the fact that introduction of niobium doping at 0.04 at. % into the TiO$_2$ band gap may have induced a red shift in the band gap transition and therefore enhances visible light absorption. This could be due to an increase in charge transfer between the niobium dopant and the TiO$_2$ conduction band or a d–d transition/interaction in the crystal field at this optimal niobium doping concentration (Choi *et al*, 1994)
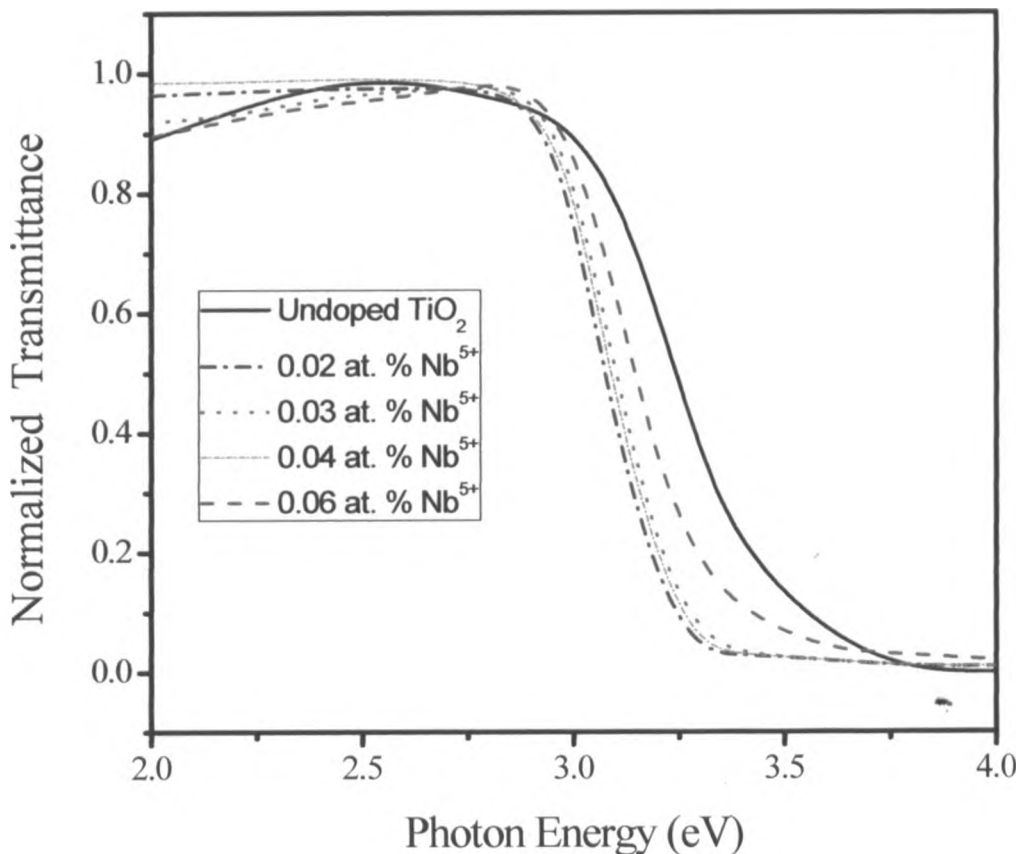
Fig. 5.4: Normalized transmittance versus energy (eV) for Nb–doped TiO$_2$ films at 0.02, 0.03, 0.04, 0.06 at. % Nb^{5+} concentrations and un–doped TiO$_2$ films.

In figure 5.5, the corresponding spectral dependencies of $\alpha^2(E)$ in arbitrary units have been plotted against photon energy (E) to find the values of the band gaps (E_g) for all

the prepared samples and the un–doped TiO$_2$. It is seen from the low niobium doping range of 0.02–0.06 that the band gap decreases as the Nb^{5+} concentration increases, reaching a minimum band gap at 3.017 eV for Nb^{5+} concentration of 0.04 at. % Nb^{5+} and starting to increase again at 0.06 at.% Nb^{5+}. Inset, the extrapolations for the plots $\alpha^2(E)$ versus E for Nb^{5+} concentration of 0.04 at. % and 0.06 at. % has been magnified for clarity. The band gaps corresponding to these two Nb–doping concentrations in TiO$_2$ are 3.017 and 3.036 eV respectively.
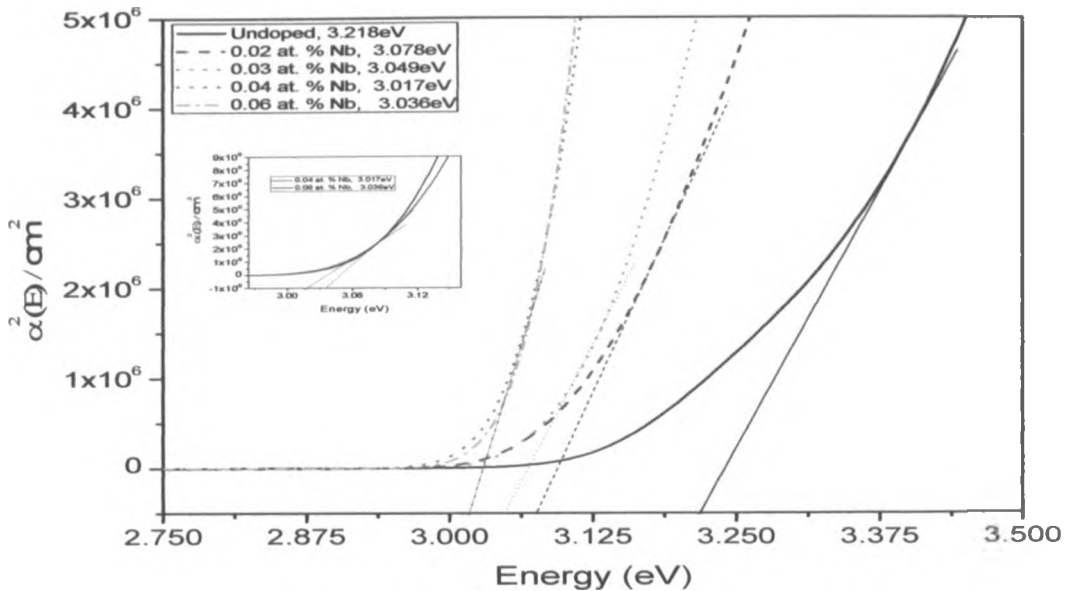
Fig.5.5: Absorption coefficient squared in arbitrary units versus photon energy for .02, 0.03, 0.04, 0.06 at. % Nb^{5+} and un–doped TiO$_2$ (solid–line).

Pure TiO$_2$ has optical absorption edge of 3.218 eV (394 nm), while at our doping concentration of 0.04% Nb^{5+}, an optical absorption edge of 3.017 eV (412.2 nm) was obtained resulting into a red shift of 0.181 eV (18.2 nm) into the visible spectrum (Fig. 5.5).

obtained resulting into a red shift of 0.181 eV (18.2 nm) into the visible spectrum (Fig. 5.5).

Figure 5.6 shows the dependence of optical band gap (eV) on % Nb^{5+} concentration which further confirms the observations in Fig 5.5. The figure shows that Nb–doping affects light absorption characteristics of TiO_2. As the niobium concentration increases at the Nb–doping range studied, the optical band gap has a decreasing trend and starts to increase again. From the figure, (drawn from Table 5.2), a minimum band gap was obtained at 0.04 at. % Nb^{5+}. This may suggest that at this concentration there was a maximum substitution of Nb^{5-} on Ti^{4-} lattice sites. This results in creation of an equal amount of Ti^{3-} ions in order to compensate for the substitution, and this further reinforces the consideration of Nb as a donor dopant in TiO_2 (Feroni et al, 2000).

Table 5.2: Calculated at. % Nb^{5+}, average crystallite sizes, and optical band gap of the Nb–doped TiO_2

At.% Nb^{5+}	Average crystallite size (nm)	Optical band gap (eV)
0.02	41.407	3.078
0.03	43.141	3.049
0.04	39.923	3.017
0.06	41.604	3.036
Un-doped	125.157	3.218

From Table 5.2, the results show that except for Nb–concentration of 0.03 at. %, as the particle sizes decrease, the optical band gap decreases from 3.218 eV to 3.017 eV with a resultant shift of the optical absorption edge into the visible light region. The optical band gap increases again from 3.017 eV to 3.036 eV as the particle sizes starts to increase again. This observation may be explained in terms of the higher ordered nature (slight yellow colour) of the TiO_2 introduced by the niobium doping.
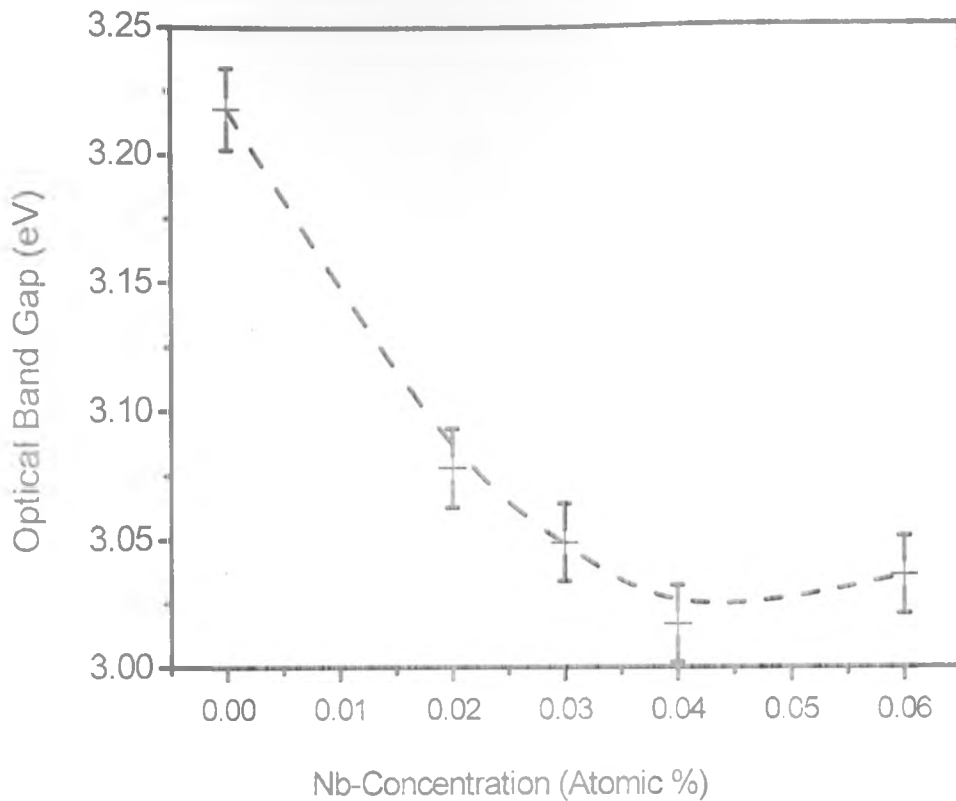
Fig.5.6: Optical band-gap energy ($\pm$ 0.5 eV) versus niobium ion concentration (Nb^{5+} at. %).

The result of band gap change as a function of particle size was also observed by Lin *et al*, 2006. They obtained a decrease in optical band gap from 3.289 eV to 3.173 eV when the particle size decreased from 29 nm to 17 nm.

Since the ionic radius of Nb^{5+} (0.69 Å) is fairly comparable to that of Ti^{4-} (0.64 Å) it was expected that solubility of niobium in TiO_2 phases induced minimum stress. Hence the most probable model of doping would be a substitutional one with Nb^{5-} in Ti^{4+} positions with subsequent formation of cation vacancies (**V**) to maintain charge neutrality of the overall stoichiometry (Andreas *et al*, 2006). Furthermore, since Nb^{5+} has a higher valency than Ti^{4+}, it acts as a donor atom when dissolved in TiO_2 because of charge transfer from the Nb 5s derived state to the conduction band. At the investigated Nb–dopant concentration (0.02–0.06 at. %), a minimum band gap of 3.017 eV (412.2 nm, and 18.2 nm red shift into the visible spectrum) was obtained at

dopant concentration of 0.04 at. % Nb^{5+}. This represented a band gap lowering of approximately 0.181 eV.

CHAPTER SIX

CONCLUSION AND SUGGESTIONS FOR FURTHER WORK

6.1 Conclusion

The following are the main conclusions:

1. We attempted to fabricate Nb–doped TiO_2 thin films via high temperature diffusion for possible applications in various photochemical fields. Within the investigated niobium doping range of 0.02–0.06 at. %, calcined at 850 $^{\circ}$C for 5 hours, the sample with 0.04 at. % Nb^{5+} gave an optimum absorption. At this concentration, a minimum optical band gap of 3.017 eV was obtained, i.e., a red shift of 18.2 nm into the visible spectrum resulting into a band gap lowering of 0.181 eV. The Nb–doped films absorb more of the visible light than the un–doped TiO_2 and appeared yellowish, which was attributed to O–Nb=O centres in agreement with results of Andreas *et al.* (2006).

2. Doping of TiO_2 with cations such as Nb^{5+} of valence higher than that of the parent cation (Ti^{4+}) enhances its visible light absorption. At the investigated Nb–doping range, it was noted that the visible light absorption efficiency goes through a maximum (0.04 at. % Nb^{5+}) with increasing dopant concentration in the TiO_2 matrix. This optimal niobium doping concentration, resulted in 412.2 nm optical absorption edge, and this was fairly above the optical absorption edge of pure (undoped) TiO_2 (394 nm).

3. The band gaps which were obtained from the transmittance data via the square of absorption coefficient (α) versus photon energy ($h\nu$) plots indicated that beyond the niobium dopant concentration of 0.04 at. % in TiO_2, the width of the optical band gap starts to increase again (3.036 eV at 0.06 at. % Nb^{5+}). Hence, at the Nb–dopant concentration range studied, there appears to be an optimal niobium concentration beyond which the absorption of Nb–doped TiO_2 decreases. The variations in optical band gaps due to Nb–doping are explained in terms of the formation of new electronic states due to the donor-behavior of niobium.

4. The Nb–doped films produced an average transmittance of approximately 60 % and very low reflectance of less than 10 %. At the investigated niobium concentrations range of 0.02–0.06 at. % the transmittance of the films were generally found to increase with increase in niobium concentration. The transmittance spectra of Nb–doped films showed a shift of absorption beginning at 412 nm (3.017 eV) for the optimum niobium doping concentration of 0.04 at. %. Nb^{5+}. The result matches closely with that of Saila Karvinen, 2003 who obtained a sharp absorption at 413 nm (3.00 eV) for 0.027 at. % Nb^{5-}.

5. From the XRD results, the calculated average particle sizes were found to range from 39.923 to 43.141 nm. Hence, we can conclude that Nb–doping seem to have a clear influence on particle morphology and specific surface area. These results and others in literature (Wang *et al*, 1994; Lin *et al*, 2006), suggest that there is a relationship between niobium dopant concentration in TiO_2 and the resultant crystallite sizes. The relatively high percentage of rutile phase displayed by the X–ray diffractograms give valuable information of the inability of such low Nb–doping as anatase–rutile phase transformation inhibitor at our doping temperature of 850 °C.

6. The results show that the investigated low Nb–doping range (0.02–0.06 at. % can be used to improve the optical characteristics and crystal structure of TiO_2 for possible technological applications in either gas sensors or solar cells.

6.2 Suggestions for Further Work

It is an intricate matter to introduce Nb–dopant into TiO_2 lattice in order to alter its optical band gap energy. The high temperature diffusion used (850 °C) may not have produced high quality films for a wide range of applications. Existence of impurity mixed TiO_2 and Nb_2O_5 powders cannot be ruled out due to incomplete diffusion of niobium into the TiO_2 lattice. Further studies on the use of higher temperatures (> 850 °C) with variable calcinations times to ensure complete diffusion of Nb into TiO_2 while at the same time ensuring thermal stability of the films is still required. This will result into getting a compromise phase transformation mechanism.

In this study, the Nb–doped TiO_2 colloidal solutions used to prepare the films were ground manually using an agate mortar. This may not have resulted in obtaining ideal nano–sized colloids best suited to investigate the influence of Nb–doping on the optical and strucural characteristics of TiO_2. An aluminium ball mill or a three–roll mill would be most recommended for the preparation of a more reliable nano–sized Nb–doped TiO_2 colloids.

The study explored the influence of concentration of dopant states of niobium on the optical and structural properties of Nb–doped TiO_2 at very low doping levels (range of 0.02–0.06 at. % Nb^{5+}). A wider and even higher Nb–doping concentration ranges need to investigated in order to obtain further conclusions on better technological fabrications of Nb–doped TiO_2 photoelectrodes for future applications.

REFERENCES

Anpo M., Ichihashi Y., Takauchi M. and Yamashita H. (1998), *Res. Chem. Intermed*, **24**, no. 143, pp. 273–279.

Anukuprasert T., Saiwan C. and Traversa E. (2005), The Development of Gas Sensor for Carbon Monoxide Monitoring using Nanostructure of Nb–TiO₂, *Science and Technology of Advanced Materials*, **6**, pp. 359–363.

Arbiol J., Gerdi J, Dezannaan G., Cireva A., Peiro F., Cornet A. and Morante J. F. (2002), Effects of Nb–doping on the TiO_2 anatase–to–rutile phase transition, *Applied Physics Letters*, **92**, no. 2, pp. 853–861.

Asahi R., Morikawa T., Aoki K., Ohwaki T. and Taga Y. (2001), Visible–light Photocatalysis in Nitrogen–doped Titanium oxide, *Science*, **293**, no. 5528, pp. 269–271.

Ayllon Jose A., Ana M. Pairo, Lahcen Saadoum, Elena Vigil, Xavier Domenech and Jose Peral (2000), Preparation of anatase powders from fluorine–complexed titanium (IV) aqueous solution using microwave irradiation, *Journal of Materials Chemistry*, **10**, pp. 1911–1914.

Banerjee S. K. (2002), Solid State Electronic Devices, Fifth Edition, pp. 62–64 and 108–111.

Boer K.W. (1991), A Survey of Semiconductor Physics, **II** pp. 963–997.

Boerasu I., Pereira M., Gomes M. J. M. and Ferreira M. I. C. (2000), Structural and Optical Characterization of Nb–doped PZT 65/35 Thin Films Grown by Sol–gel and Laser Ablation Technique, *Journal of Optoelectronics and Advanced Materials*, **2**, no. 5, pp.602–609.

Bonini N., Carrota M.C., Chiorino A., Guidi V., Malagu C., Martinelli G., Paglialonga L. and Sacardoti M. (2000), Doping of a Nanostructure Titania Thick

Films: Structural and Electrical Investigations, *Sensors and Actuators B*, **68**, pp. 274–280.

Borgarello E., Kiwi J., Gratzel M., Pelizzetti E. and Visca M. (1982), Visible Light Induced Water in Colloidal Solutions of Chromium Doped Titanium Dioxide Particles, *Journal ofAmerican Chemical Society*, **104**, pp. 2996–3004.

Choi Woyong, Andreas Tarmin and Michael R. Hoffman (1994), The role of Metal Ion Dopants in quantum–sized TiO_2: Correlation between Photoreactivity and Charge Carrier Recombination Dynamics, *Journal of Physical Chemistry*, **98**, pp. 13669–13679.

Cristiana Di Valentin, Gianfranco Pacchioni and Aunabella Selloni (2004), Origin of the different Photoactivity of N–doped anatase and Rutile TiO_2, *Physical Review B*, **70**, no. 08511, pp. 1098–1121.

Diwald Oliver, Tracy L. Thompson, Tykhom Zubkou, Goralski G. Ed., Scott Walck D. and John T. Yates Jr. (2004), Photochemical Activity of Nitrogen-Doped Rutile TiO_2 (110) in Visible Light, *Journal of Physical Chemistry B*, **108**, pp. 6004–6008.

Edelson L. H. and Glaeser A. M. (1988), Role of particle substructure in the phase transformation of TiO_2 at high temperatures, *Journal of American Ceramic Society*, **71** p. 225–235.

Feroni M., Carotta M. C., Guidi V., Martinelle G., Rouconi F., Richard O., Van Dyck D. and Landuyi Van J. (2000), Structural Characterization of Nb–TiO_2 nanosized thick Films for Gas Sensing Applications, *Sensors and Actuators B*, **68**, pp. 140–145.

Fujishima A., Rao N. T. and Tryk A. D. (2000), Titanium Dioxide Photocatalysis, Journal of Photochemistry and Photobiology C: *Photochemitry Review*, **1**, pp. 1–21.

Gratzel M. (1983), Energy Resources through Photochemistry and Catalysis, *Academic Press*, New York.

Grätzel M. (2003), Dye–Sensitized Solar Cells, *Journal of Photochemistry and Photobiology C: Photochemistry Reviews*, **4**, pp. 145–153.

Grätzel M. and O'Regan B. (1991), A Low–cost High Efficiency Solar Cell based on Dye– sensitized Colloidal TiO_2 Films, *Nature*, **353**, pp. 737–739.

Hagfeldt and Grätzel M. (1995), Light–Induced Redox Reactions in Nanocrystalline Systems, *Chemistry Review,* **95**, no.1, pp. 49–68.

Hague D. C. and Mayo I. M. (1993), Effect of crystallization and a phase transformation of TiO_2 calcined at high temperatures, *Nanostructured Materials*, **3**, no. 1–6, pps. 61.

Hattori A., Shimoda K., Tada H. and Ito S. (1999), Photoreactivity of Sol–gel TiO_2 Films formed on Soda–lime Glass Substrates: Effect of SiO_2 Underlayer Containing Fluorine, *Langmuir*, **15**, no. 16, pp. 5422–5425.

Karakitsou Kyriaki E. and Verykios Xenophon E. (1993), Effects of Altervalent Cation Doping of TiO_2 on its Performance as a Photocatalyst for Water Cleavage, *Journal of Physical Chemistry,* 97, pp. 1184–1189.

Karvinan Saila M. (2003a), The Effects of Trace Elements on the Crystal Properties of TiO_2, *Solid State Sciences*, **5**, pp. 811–819.

Karvinen Saila M. (2003b), The effects of Trace Element Doping on the Optical Properties and Photocatalytic Activity of Nanostructured Titanium Dioxide, *Industrial Engineering Chemistry Research,* **42**, pp. 1035–1043.

Lin H., Huang C. P., Li W., Shah Ismart H. and Tseng Yao-Hsuan (2008), Size Dependency of Nanocrystalline TiO2 on its Optical Property and Photocatalytic Reactivity Exemplified by 2-Chlorophenol. *Applied Catalysis B:Environmental*, **68**, pp. 1–11.

Lindgren T., Mwabora M. J., Avandamo E., Johnson J., Hoel A., Granquist G. C. and Lindquist E. S. (2003), Photoelectrochemical and Optical Properties of Nitrogen Doped TiO₂ Prepared by Reactive D.C. Magnetron Sputtering, *Journal of Physical Chemistry B*, **107**, pp. 5709–5713.

Liu F. M., and Wang M. T. (2002), Surface and Optical Properties of Nanocrystalline Anatase Titania Films grown by Radio Frequency Reactive Magnetron sputtering, *Applied Surface Science*, **195**, pp. 284–290.

Madare Diana, Tasca M., Delibas M. and Rusu G. I. (2000), On the Structural Properties and Optical Transmittance of TiO₂ r. f. Sputtered Thin Films, *Applied Surface Science*, **156**, pp. 200–206.

Martin S.T., Herman H., Choi W. and Hoffman M. R. (1997), *Journal of American Chemical Society*, Faraday Transport in Press.

Mattson Andreas, Michael Leideborg, Karin Larsson, Gunner Westin and Lars Osterlund, (2006), Absorption and Solar Light Decomposition of Acetone on Anatase TiO₂ and Niobium Doped TiO₂ Thin films, *Journal of Physical Chemistry B*, **110**, pp.1210–1220.

Minaro M., Fox A. and Draper B. R. (1989), Changes in Microstructural Characteristics of Degussa P–25 Titania as a Result of Calcinations, *Langmuir*, **5**, pp. 250–255.

Miyagi Takahira, Masayuki Kamei, Lsao Sakaguchi, Takefumi Mitsuhashi and Atushi Yamashaki (2004), Photocatalytic Property and Deep Levels of Nb–doped Anatase TiO₂ Film Grown by Metalorganic Chemical Vapour Deposition, *Japanese Journal of Applied Physics*, **43**, no. 2, pp. 775–776

Mizushima K., Tamaka M., Asai A., Iida S. and Goodenough B. J. (1979), Solids, *Journal of Physical Chemistry B*, **40**, pp. 1129–1133.

Moser J., Punchihewa S., Infelta P. P. and Grtzel M. (1991), Solar Energy Conversion in electron transfer in Chemistry, *Langmuir*, 7 no. 12, pp. 3012–3018.

Niishiro Ryo. Hideki Kato and Akihiko Kudo (2005), Nickel and Either Tantalum or Niobium Co-doped TiO_2 and $SrTiO_3$ Photo-catalysts with Visible Light Response for H_2 or O_2 Evolution from Aqueous Solutions. *Research paper*. pp. 1–8.

Ohtsuka Y., Fijiki Y. and Suzuki Y. (1982), *Journal of Japanese. Association of Mineral, Petrolium and Geology*, 77, pp. 117–126.

Porter John F., Yu-Guang Li and Chak K. Chan (1999), The Effect of Calcination on the Microstructural Characteristics and Photoreactivity of Degussa P–25 TiO_2, *Journal of Materials Science*, 34, pp. 1523–1531.

Qamar M., Muneer M. and Bahnemann D. (2006), Heterogeneous Photocatalysed Degradation of Two Selected Pesticide Derivatives. Triclopir and Daminozid in Aqueous Suspensions of Titanium Dioxide, *Journal of Environmental Management*, 80, pp. 99–106.

Redecka M., and Rekas (1995), The studies of High Temperature Interaction of Nb–TiO_2 Thin Films with Oxygen, *Journal of Physical Chemistry of Solids*, 56, no. 8, pp. 1031–1037.

Rodriguez M. J., Gomez Ederth J., G.A. Niklasson A. G. and Granquist G. C. (2000), Thickness Dependence of the Optical Properties of Sputter Deposited Ti Oxide Films, *Thin Solid Films*, 365, pp. 119–125.

Ruiz A., Dezanneau G., Arbiol J., Cornet A. and Morante J. R. (2003). Study of the Influence of Nb Content and Sintering Temperature on TiO_2 Sensing Films, *Thin Solid Films*, 436, pp. 90–94.

Schmitt M. and Aegerter A. M. (2001), Electronic Properties of Pure and Doped Nb_2O_5 Coatings and Devices, *Electrochemical Actuators*, 46, pp. 2105–2111.

Sclafani A., Palmisano L. and Schiavello M. (1990), Influence of the preparation method of TiO_2 on the photocatalytic properties of Degussa P–25. *Journal of Physical Chemistry,* **94,** no. 2, pp.829–832.

Scotter E., Vilanova X., Llobet E., Stankova M. and Correig X. (2005), Niobium–doped Titania Nanopowders for Gas Sensor Applications. *Journal of Optoelectronic and Advanced Materials,* **7,** no. 3. pp. 1395–1398.

Sheppard L. R., Bak T., Nowotny J. and Nowotny K. M. (2008), Effect of Oxygen Activity on Niobium Segregation in Niobium doped Titanium Dioxide. *Journal of the Australian Ceramic Society,* **44,** no. 2, pp. 42–46.

Shinde Pravin S., Pramod S., Patil Popat, Bhosale N. and Chandrakant H. Bhosale (2008), Structural, Optical, and Photoelectrochemical Properties of Sprayed TiO_2 Thin films: Effects of precursor concentration, *Journal of American Chemical Society,* 91, no. 4, pp. 1266–1272.

Smestad G. (1998), Education and Solar Energy Conversion: Demonstrating Electron Transfer. *Solar Energy Materials and Solar Cells,* **55,** pp. 157–178.

Sodergren S., Hagfeldt A., Olsou J. and Lindquist E. S. (1994), Theoretical Models for the Action Spectrum and the Current Voltage Characteristics of Microporous Semi-Conductor films in Photoelectrochemicall Cells. *Jounal of Physical Chemistry B,* **98.** pp. 5552–5556.

Soonchul Kwon, Maohong Fan, Adrienne Cooper and Hongqun Yang (2008), Photocatalytic Applications of Micro–and Nano–TiO_2 in Environmental Engineering, *Critical Reviews inEnvironmental Science and Technology,* **38** (3), pp. 197–226.

Tang H. Berger, Achmid P. E. and Levy F. (1994), Optical Properties of anatase TiO_2, *Journalof Solid State Chemistry,* **92,** pp. 267–274.

Thevuthasan S., Shivaparan R. N., Smith J. R., Gao Y. and Chambers A. S. (1997), Rutherford Backscattering and Channeling Studies of a TiO_2 (100) Substrate

Epitaxially Grown Pure and Nb–doped TiO_2 films, *Applied Surface Science*, 115, pp. 38–385.

Titanium dioxide–Wekipedia, the free Encyclopedia. web page: *http://en.wikipedia.org/wiki/Titanium-dioxide*

Todorova N., Giannakopoulou T., Romanos G., Vaimakis T., Jiaguo Yu and Trapalis C. (2007), Preparation of Fluorine–Doped TiO_2 Photocatalysts with Controlled Crystalline Structure, *International Journal of Photoenergy*, 2008, Research Article. pp. 1–9.

Trenczek–Zajac Anita, Marta Radaka and Mieczyslaw Rekas (2007), Photoelectrochemical Properties of Nb–doped Titanium dioxide. *Physica B.*, 399, pp. 55–59.

Tyagi M. S. and Sharma B. L. (1984), In Metal Semiconductor Schottky Barrier Junctions and their Applications, *Plenum Press*, New York.

Umebayashi T., Yamaki T., Sumita T. and Asai K. (2003a), Sulphur–doping of rutile–titanium dioxide by ion implantation: Photocurrent spectroscopy and first–principle band calculation studies, *Journal of Applied Physics*, 93. no. 9. pp. 5156–5160

Umebayashi T., Yamaki T., Sumita T., Yamamoto S., Tamaka S. and Asai K. (2003b), UV- ray photoelectron and ab initio band calculation studies on electronic structures of Cr–or Nb–ion implanted titanium dioxide. *Nuclear Instruments and Methods in Physics Research B*, 206, pp. 264–267.

Umebayshi T., Yamaki T., Itoh H. and Asai H. (2002), Band Gap Narrowing of Titanium Dioxide by Sulphur Doping, *Applied Physics Letters*, 81. no. 3. pp. 454–455.

Wang Hao and Lewis James P. (2005), Effects of Dopant States on Photoactivity in Carbon- doped TiO_2, *Journal of Physics: Condensed Matter*, 17, pp. 209–213.

Yamada Yasushi, Yoshiki Semo, Yumi Masuoka, Tadashi Nakamura and Katsuji Yamashita (2000), NO$_2$ Sensing Characteristics of Nb-doped TiO$_2$ thin films and their electronic properties, *Sensors and Actuators B*, **66**, pp. 164–166.

APPENDIX I

Sample calculation of at. % Nb–doped in TiO_2

Let $0.01g$ of Nb_2O_5 be mixed with $10g$ of TiO_2

The formula. mass of $Nb_2O_5 = 265.80976g$ (2 moles of Nb^{5+})

Hence $265.80976g$ contains $2 \times 6.02 \times 10^{23}$ ions of Nb^{5+}

where 6.02×10^{23} is the Avogadro's constant.

$$\therefore 0.01g = \frac{0.01}{265.80976} \times 2 \times 6.02 \times 10^{23}$$

$$= 4.529555 \times 10^{19} \text{ ions of } Nb^{5+}$$

The formula mass of $TiO_2 = 79.8788g$ (1 mole of Ti^{4+} and 2 moles of O^{-})

Hence $79.8788g$ contains $3 \times 6.02 \times 10^{23}$ ions of Ti^{4+} and O^{2-}

$$\therefore 10g = \frac{10}{79.8788} \times 3 \times 6.02 \times 10^{23}$$

$$= 2.260925 \times 10^{23} \text{ ions of } Ti^{4+} \text{ and } O^{2-}$$

So, the % of Nb^{5+} dopant to Ti^{4+} and O^{2-} on an ion basis is given by:

$$\frac{4.529555 \times 10^{19}}{2.260925 \times 10^{23}} \times 100 = 2 \times 10^{-2} = 0.02 \text{ at. % of } Nb^{5+}$$

APPENDIX II

Physical and Chemical Properties of TiO_2

    a) **Physical properties:**

        1. Colour :   White powder

        2. Molecular mass (Formula mass) : $79.8788g$

        3. Boiling point at sea level : $2500\,^{\circ}C$

        4. Specific gravity near room temperature: 3.9 at $20\,^{\circ}C$. ($68\,^{\circ}F$)

        5. Vapour density :   Not applicable

6. Solubility: Insoluble in water

7. Evaporation rate: Not applicable

b) **Chemical properties:**

1. Combustibility: Non–combustible

2. Smell: Odorless

3. Reactivity: Reacts violently with Lithium at 200 °C

4. Instability conditions : Not applicable

5. Hazards :   None reported

6. Special precautions : None

APPENDIX III

Physical, Atomic and Chemical Properties of Niobium

a) **Physical properties:**

1. Phase : solid

2. Density near room temperature : 8570kg/m

3. Melting point : 2477 °C, 2750 K

4. Boiling point : 4744 °C, 5017 K

5. Heat of fusion : 30 KJmol

6. Heat of vaporization : 689.9 KJmol^{-1}

7. Specific heat capacity : 24600KJmol^{-1}K

b) **Atomic properties:**

1. Name, symbol, number : Niobium, Nb, 41

2. Element category : Transition metal

3. Group, period, block : 5, 5, d

4. Standard atomic weight : 92.90638kgm

5. Oxidation state : 5, 4, 3, 2, -1

6. Electro negativity : 1.6 (Pauling scale)

7. Ionization energies : 1st: 652.1 KJmol^{-1}

$\qquad\qquad\qquad\qquad$ 2nd: 1380 KJmol^{-1}

$\qquad\qquad\qquad\qquad$ 3rd: 2416 KJmol^{-1}

9   Atomic radius: 1.46Å

8. Covalent radius : 1.64 ± 6Å

c) **Chemical properties:**

1. Smell :   Odorless
2. Solubility :   Insoluble in water
3. Combustibility : Non-combustible
4. Reactivity: Reacts with dilute acids to form salt and water.

APPENDIX IV
Physical and Chemical Properties of Nb_2O_5

a) **Physical properties:**

1. Molecular weight: 0.26580976 kg/mol
2. Apparent density: 4470kg/m^2
3. Bulk density: 4470kg/m^3
4. Melting point: 1520 °C

b) **Chemical properties:**

1. Smell: Odorless
2. Solubility: Insoluble in water
3. Combustibility: Non-combustible
4. Reactivity: Reacts mildly with bases to form complex salts